

A PENALTY FINITE ELEMENT MODEL FOR AXISYMMETRIC
FLOWS OF POWER-LAW AND WHITE-METZNER FLUIDS

by

V. A. Padhye

Thesis submitted to the Faculty of the
Virginia Polytechnic Institute and State University
in partial fulfillment of the requirements
for the degree of

MASTER OF SCIENCE

in

Engineering Mechanics

APPROVED:

J. N. Reddy, Chairman

D. G. Baird

D. T. Mook

November 1986
Blacksburg, Virginia

A PENALTY FINITE ELEMENT MODEL FOR AXISYMMETRIC
FLOWS OF POWER-LAW AND WHITE-METZNER FLUIDS

by

V. A. Padhye

ABSTRACT

A finite element model based on the penalty function formulation of the equations governing unsteady axisymmetric flows of viscous incompressible fluids obeying power-law and White-Metzner constitutive relations is developed. The formulation accounts for inertial (or convective) terms. For power-law fluids, two different finite element models are developed: one based on the velocity formulation (i.e., only velocities as nodal variables) and the other based on a mixed formulation involving velocities and stress components. For the White-Metzner model, only the mixed model involving the velocities and extra stress components can be developed. The pressure variable does not enter the finite element model because of the application of the penalty method to introduce the incompressibility constraint. However, the pressure can be post-computed once the velocities are obtained.

The finite element models are used to analyze several plane and axisymmetric flows of power-law and White-Metzner fluids. The effect of boundary conditions, power-law model, inertia terms on the velocity profiles is investigated. The numerical solutions agree, qualitatively, with the known experimental and numerical results. The finite element models developed here can be easily modified to include thermal effects and other constitutive models.

ACKNOWLEDGEMENTS

The author wishes to express her gratitude and appreciation to Dr. J. N. Reddy for his excellent guidance and expert advise.

She also wishes to thank the members of her examining committee, Dr. Mook and Dr. Baird for their valuable suggestions.

The support of this research through a research grant to Professors J. N. Reddy and D. G. Baird by the Center for Innovative Technology (CIT) at Virginia Polytechnic Institute and State University is gratefully acknowledged. It is also a pleasure to acknowledge the skillful typing of this manuscript by Mrs. Vanessa McCoy.

The author greatly appreciates and thanks her mother-in-law, Mrs. Pratima Padhye, and husband, Atul, for their love, support and encouragement. I hope to make up for the time I missed with my children Avishkar and Anubhav, because of my occupation with this research.

TABLE OF CONENTS

	Page
CHAPTER I: INTRODUCTION.....	1
1.1 General Comments.....	1
1.2 Various Formulations of Fluid Flow.....	2
1.3 Numerical Models of Non-Newtonian Fluids.....	4
1.4 Objectives of the Present Study.....	7
CHAPTER II: GOVERNIG EQUATIONS.....	8
2.1 Equations of Motion and Continuity.....	8
2.2 Constitutive Equations.....	8
2.2.1 Power-Law Model.....	9
2.2.2 The White-Metzner Model.....	9
2.3 Specialization to Axisymmetric Flows.....	11
CHAPTER III: FINITE ELEMENT MODEL.....	14
3.1 The Penalty Function Formulation.....	14
3.1.1 Plane Flow.....	15
3.1.2 Axisymmetric Flow.....	16
3.2 Finite Element Models.....	17
3.2.1 Plane Flow.....	17
3.2.2 Axisymmetric Flow.....	19
3.3 Boundary Conditions.....	20
3.4 Time Approximations.....	21
3.5 Iterative Technique.....	22
CHAPTER IV: NUMERICAL RESULTS.....	23
4.1 Preliminary Comments.....	23
4.2 Discussion of the Results.....	23
4.2.1 Effect of Mesh.....	23
4.2.2 Effect of Stress Boundary Conditions.....	29
4.2.3 Effect of Inertia.....	32
4.2.4 Effect of Penalty Parameter.....	32
4.2.5 Analysis of Power-Law Fluids.....	35
4.2.6 Analysis of White-Metzner Fluids.....	46
4.2.7 Transient Analysis.....	62
CHAPTER V: CONCLUSIONS AND RECOMMENDATIONS.....	69
4.1 Conclusions.....	69
4.2 Recommendations.....	69
REFERENCES.....	71
APPENDIX A: Matrix Coefficients for Plane Flow.....	75
APPENDIX B: Matrix Coefficients for Axisymmetric Flow.....	79
VITA.....	84

NOMENCLATURE

a, b, c	Constants of polymeric melts
I_i	Invariants of rate of deformation tensor
$[K^e]$	Element stiffness matrix
$[M^e]$	Element mass Matrix
n	Power law index
P	Pressure
r, z	Radial and axial coordinates, respectively
t	Time
u, v, w	Velocity components in y, t and z coordinate directions, respectively
u_j, v_j, w_j	Nodal velocities
u_i	Velocity of fluid in i th direction
τ_{ik}^j	Nodal extra stress components
$\underline{\tau}$	Extra stress tensor
$\underline{\tau}^1$	Viscoelastic part of extra stress tensor
$\underline{\tau}^2$	Purely viscous part of extra stress tensor
$\underline{\gamma}$	Rate of deformation tensor (or strain rate tensor)
γ	Shear rate
η_0	Initial viscosity
η	Shear viscosity
η_1, η_2	Fractions of shear viscosity
λ	Relaxation time
γ_p	Penalty parameter
δ	Variational symbol
Ω^e	A typical finite element

Γ^e	Boundary of Ω^e
ψ_j	Interpolation functions
α	Parameter in the the time approximation
β	Acceleration parameter
θ	Angular coordinate

CHAPTER I

INTRODUCTION

1.1 General Comments

Some of the most challenging and important areas currently under investigation in computational fluid mechanics concern finite element analysis of flows of non-Newtonian fluids. A Non-Newtonian fluid is defined to be the one whose constitutive behavior is nonlinear (i.e., stresses are nonlinearly related to strains). Such fluids may or may not have memory of past deformation (i.e., viscoelastic or not). Practical examples of such fluids are multigrade oils, liquid detergents, paints, and printing inks. Polymer solutions and polymer melts also fall within this category. All such flows are extremely important in forming processes of various kinds applied to metals, plastics or glass. The advent of computers and powerful numerical methods has created considerable interest in the analysis of flows of such fluids.

Although most of these flows are fully three-dimensional and time dependent, the limitations imposed by both experimental and theoretical techniques have forced researchers to analyze only those fluid motions that are believed to render themselves to approximation by two-dimensional models. The Navier-Stokes equations describing these phenomena are highly nonlinear, and the strong coupling between the equations make it difficult to obtain analytical solutions.

Recent advances in computer hardware have made it possible to investigate several finite difference and finite-element formulations of

the Navier-Stokes equations. One of the major difficulties associated with the solution of Navier-Stokes equations in non-rectangular geometries is the application of boundary conditions. Although attempts have been made to rectify this problem by constructing body fitted curvilinear meshes in finite difference methods, the finite element method has a definite advantage in that any complicated geometry can be suitably represented by using non-uniform and non-rectangular meshes, and appropriate body conditions of the model can be imposed in a natural way. Much of the earliest work in the finite element analysis of fluid flow was primarily in the area of porous media (see Zienkiewicz and Cheung [1]) and potential flows, which are considered to be simple extensions of the procedures developed in linear elasticity. Early applications of the finite element method in the numerical solution of the Navier-Stokes equations governing viscous, incompressible fluids can be found in the works of Oden and his colleagues [2-4], Argyris, et al. [5], Tong [6], Cheng [7], Olson [8], Baker [9,10], Taylor and Hood [11], and Kawahara, et al. [12], among others.

1.2 Various Formulations of Fluid Flow

The finite element models of the two-dimensional Navier-Stokes equations have been based on four basic formulations described in the paragraphs below.

Stream function-vorticity model. Most studies using finite difference methods follow the stream function-vorticity approach. The finite-element model based on this approach has been employed by Cheng [7], Olson [8,13], and by others. In this model, boundary conditions on

the vorticity are computed from the stream function at the boundary. However, this leads to large errors in the vorticity (see, Davis [14]) for advection dominated flows.

Stream function model. Finite-element models based on this approach can be found in the works of Olson and his colleagues [8, 15]. Due to the higher-order nature of the equation, the associated finite element model is algebraically complex. Due to the similarity of the stream function equation to that of the biharmonic equation governing the transverse deflection of a plate, a plate bending finite-element program can be modified to solve the flow problem.

Velocity-pressure model. This is the most natural and direct formulation, which is also known as the mixed formulation. The model is based on the Navier-Stokes equations and the continuity equations, all expressed in terms of the primitive variables (u,v,P) (see Taylor and Hood [11], Olson and Tuann [15], Reddy [16,17]).

Penalty function model. The penalty function model is also based on the primitive variable equations, except that the continuity equation is treated as a constraint on the velocity field. The constraint is introduced into the finite-element model by means of the penalty function method (Zienkiewicz [18], Hughes et al. [19], and Reddy [17,20-22]). Details of the formulation will be discussed later.

Each of the formulations has certain relative advantages and disadvantages. The velocity-pressure formulation is the most direct and natural one in that all the variables are physical. However, the resulting finite element model is non-positive-definite. This is a direct consequence of the continuity condition, which stands uncoupled

from the momentum equations. The stream function formulation is attractive in problems where description of the flow phenomena is important. The formulation also results in positive-definite system of equations. Since the governing equation (for the stream function) is of fourth order, C^1 - continuity of the approximating functions is required (analogous to the plate bending elements). This results in algebraically complex elements and hence, large computational efforts. The stream function-vorticity formulation suffers from the drawback of requiring boundary conditions on the vorticity, which is unknown a-priori (and not independent of the stream function). However, it is convenient to describe the flow phenomena with the aid of the stream function and vorticity. The penalty function model is a primitive variable model which results in a positive-definite system of equations for Stokes flow. Another advantage of the model is that the pressure does not appear as a primary unknown, and an approximation to the pressure can be obtained in postcomputation.

1.3 Numerical Models of Non-Newtonian Fluids

Numerical techniques for solving the flow of non-Newtonian fluids differ very little from the ones used for Newtonian fluids. When the shear viscosity is a function of the rate of deformation tensor (i.e., for so-called power-law fluids), the equation of motion can still be written explicitly in terms of velocity components. For such fluids, the same formulations as those of the Newtonian fluids can be used. For example, the pressure-velocity and penalty finite element models [17] can be used for power-law fluids and viscoelastic fluids (see [23-

38])). The constitutive equations of a viscoelastic fluid can be described in terms of the extra stress components and are given in terms of either differential equations or as integral equations. In a differential constitutive model, the extra stress components and their derivatives are related to the velocity components and their derivatives. The differential constitutive models are relatively easier to model than the integral models. The computational models of viscoelastic fluids obeying a differential model require us to treat stress components as dependent variables along with the velocity components and pressure (see [38]).

A finite-element model based on the velocity-pressure-stress formulation for solving incompressible, viscous, free surface problems in steady axisymmetric or plane flows was developed by Nickell, et al. [25]. The model was used to solve the Newtonian die-swell problem for creeping jets, free surface tension constraints (see [25]). Later this model was modified by Tanner, Nickell and Bilger [24] to solve flows of many types of non-Newtonian fluids.

The differential constitutive equations of non-Newtonian viscoelastic fluids are coupled to the Navier-Stokes equations and hence must be independently approximated along with the other governing equations. In the method developed by Chang et al. [32], the stress tensor components are calculated by an iterative process. The flow of a Maxwell type fluid was considered by Kawahara and Takeuchi [33]. They introduced a mixed finite element model with six degrees of freedom ($u, v, P, \sigma_{11}, \sigma_{21}, \sigma_{12}$) per node. A Newton Raphson iteration technique was employed for the steady flow and the perturbation

technique was used for the unsteady flow. This method was further investigated by Crochet and Bezy [34]. They selected a method of total incompressibility which led to a very large number of variables and excessive constraints on the velocity field. Hence they concluded that this choice should be avoided in future work. They used six node triangular elements or a nine node Lagrangian element with quadratic approximation for the velocity components and linear approximation for pressure. Coleman [35] used a quadrilateral element obtained from two triangles and replaced the Newton-Raphson scheme by a successive substitution technique. Richards and Townsend [36] used eight node serendipity elements and successive substitution technique. Davies [37] suggested that mesh refinement was essential if inaccurate converged solutions were to be avoided and the question of mesh refinement and numerical errors must be given priority.

Most existing works in the finite-element analysis of viscoelastic fluids have considered different types of Maxwell/Oldroyd models, in which the viscosity and relaxation time both are constants. Further, the analyses were based on mixed formulations in which the velocities, pressure and stresses are treated as nodal variables. An important class of fluids, which are characterized by shear viscosity and elasticity require additional study from numerical simulation point of view. The viscoelastic effects along with memory effects of such flows can be studied using the White-Metzner model [39]. A White-Metzner model is a modification of the Maxwell model with variable viscosity and relaxation time. In both models the stress components are nonlinear functions of the deformation tensor.

1.4 Objective of the Present Study

A review of the literature indicates all of the previous work in the finite-element analysis of flows of viscoelastic fluids were based on velocity-pressure-stress formulation. Various alternative solution methods and elements were used with this formulation. The penalty finite element model has not been exploited in the solution of non-Newtonian fluids, especially the viscoelastic fluids. More recently, while the present study was under way, Read [40] and Gotsis [41] modified the penalty finite element model of Reddy [17] for Newtonian fluids to non-Newtonian fluids. These works considered steady, plane (two-dimensional) flows, and did not account for the time dependent and inertia (i.e., convective) terms.

The objective of the present study is to develop a penalty finite element model to analyze axisymmetric flows of power-law and viscoelastic White-Metzner type fluids, accounting for transient behavior and convective terms. Several examples are used to illustrate the validity of the numerical model. The effects of mesh, inertia and boundary conditions are also investigated. The penalty finite element model developed here is capable of solving the flow problems of the following types.

1. Plane or axisymmetric flows
2. Steady or unsteady flows
3. With or without inertia effects (i.e., with or without convective terms)
4. Newtonian, Power-Law and White-Metzner fluids

CHAPTER II

GOVERNING EQUATIONS

2.1 Equation of Motion and Continuity

The conservation of linear momentum yields The Navier-Stokes equations of motion,

$$\underline{\nabla} \cdot \underline{\tau} - \underline{\nabla} P = \rho \left(\frac{\partial \underline{u}}{\partial t} + \underline{u} \cdot \underline{\nabla} \underline{u} \right) \quad (2.1)$$

where

$\underline{\tau}$ extra stress tensor

P denotes the pressure

\underline{u} is velocity vector

ρ is the density of fluid.

The principle of conservation of mass, for incompressible fluids, yields the continuity of equation

$$\underline{\nabla} \cdot \underline{u} = 0 \quad (2.2)$$

2.2 Constitutive Equations

Constitutive equation for the flow dominated by shear viscosity is given by [36]

$$\underline{\tau} + \lambda \left\{ \frac{\partial \underline{\tau}}{\partial t} + \underline{u} \cdot \underline{\nabla} \underline{\tau} - [(\underline{\nabla} \underline{u})^t \cdot \underline{\tau} + \underline{\tau} \cdot (\underline{\nabla} \underline{u})] \right\} = 2\eta \underline{\gamma} \quad (2.3)$$

where

λ is the relaxation time

η is the shear viscosity of the fluid

$\underline{\gamma}$ is the rate of deformation tensor, $\underline{\gamma} = \frac{1}{2} [(\underline{\nabla} \underline{u}) + (\underline{\nabla} \underline{u})^t]$

Equation (2.3) is a general form of the constitutive equation for the viscoelastic fluids dominated by shear viscosity. In the present study, the White-Metzner type and power-law fluids are considered. Hence Eq. (2.3) are modified accordingly in the following sections.

2.2.1 Power Law Model

The simplest and most familiar non-Newtonian viscosity model is the power-law model which has the form

$$\eta = \eta_0 (4I_2)^{(n-1)/2} \quad (2.4)$$

where η_0 and n are constants, termed initial viscosity of the fluid and the power law index, and I_2 is the second invariant of the rate of deformation tensor, $I_2 = \frac{1}{2} \gamma_{ij} \gamma_{ij}$. For many non-Newtonian fluids, the apparent viscosity η decreases with increasing shear rate γ . These are called shear thinning fluids and have the power law index $n < 1$. Fluid with power law index $n > 1$ are called shear-thickening fluids. For such fluids η increases with increasing shear rate. The Newtonian viscosity is obtained with $n = 1$. The range of the power index is bounded below by zero due to stability considerations.

2.2.2 The White-Metzner Model

To characterize the White-Metzner fluid, it is necessary to know the viscosity curve as a function of shear rate and the first normal stress difference [42]. The extra stress tensor $\underline{\tau}$ is separated into purely viscous part $\underline{\tau}^2$ and viscoelastic part $\underline{\tau}^1$ which obeys Eq. (2.3).

$$\underline{\tau} = \underline{\tau}^1 + \underline{\tau}^2 \quad (2.5)$$

$$\underline{\tau}^1 + \lambda \left\{ \frac{\partial \underline{\tau}^1}{\partial t} + \underline{u} \cdot \underline{\nabla} \underline{\tau}^1 - [(\underline{\nabla} \underline{u})^t \cdot \underline{\tau}^1 + \underline{\tau}^1 \cdot (\underline{\nabla} \underline{u})] \right\} = 2\eta_1 \underline{\gamma} \quad (2.6)$$

$$\underline{\tau}^2 = 2\eta_2 \underline{\gamma} \quad (2.7)$$

where

$$\underline{\gamma} = \frac{1}{2} [\underline{\nabla} \underline{u} + (\underline{\nabla} \underline{u})^t] \quad (2.8)$$

and η_1 and η_2 can be defined as the fractions of the shear viscosity η . The fluid which obeys Eq. (2.5) is characterized by η_1 , η_2 , and λ which are the functions of rate of deformation tensor, $\underline{\gamma}$. Thus White-Metzner model is a modification of upper convected Maxwell model with variable viscosity and relaxation time coefficients.

In the present study the relaxation time λ is assumed to depend on the shear rate γ according to:

$$\lambda(\gamma) = a + b(\log \gamma) + c(\log \gamma)^2 \quad (2.9)$$

$$\gamma = \sqrt{4I_2}$$

All constants in Eq. (2.9) are evaluated by curve fitting data of polymeric melts [35].

Since η is dependent on the rate of deformation tensor, it is of the particular form,

$$\eta = \eta(\underline{\gamma}) = \eta(I_1, I_2, I_3) \quad (2.10)$$

where I_i are the invariants of $\underline{\gamma}$. For an incompressible fluid, we have $I_1 = \underline{\nabla} \cdot \underline{u} = 0$. Also, there is no theoretical or experimental evidence to suggest that the viscosity depends on I_3 . Thus Eq. (2.10) reduces to

$$\eta = \eta(\underline{\gamma}) = \eta(I_2) \quad , \quad I_2 = \frac{1}{2} \gamma_{ij} \gamma_{ij} \quad (2.11)$$

Though Eq. (2.11) gives the general functional form for the viscosity function, experimental observation and a theoretical basis

must be used to provide specific model for non-Newtonian viscosities. A variety of models can be used to calculate viscosity. In the present study the power law model in Eq. (2.4) is used.

Considering equation (2.5), the equation of motion for the White-Metzner viscoelastic fluids can be written as follows:

$$\underline{\nabla} \cdot (\underline{\tau}^1 + \eta_2 \underline{\gamma}) - \underline{\nabla} P = \rho \left(\frac{\partial \underline{u}}{\partial t} + \underline{u} \cdot \underline{\nabla} \underline{u} \right) \quad (2.12)$$

For simplicity, dropping the superscript 1 from $\underline{\tau}^1$, Eq. (2.12) becomes

$$\underline{\nabla} \cdot (\underline{\tau} + \eta_2 \underline{\gamma}) - \underline{\nabla} P = \rho \left(\frac{\partial \underline{u}}{\partial t} + \underline{u} \cdot \underline{\nabla} \underline{u} \right) \quad (2.13)$$

and Eq. (2.6) becomes

$$\underline{\tau} + \lambda \left\{ \frac{\partial \underline{\tau}}{\partial t} + \underline{u} \cdot \underline{\nabla} \underline{\tau} - [(\underline{\nabla} \underline{u})^t \cdot \underline{\tau} + \underline{\tau} \cdot (\underline{\nabla} \underline{u})] \right\} = 2\eta_1 \underline{\gamma} \quad (2.14)$$

Equations (2.12), Eq. (2.13) and (2.14) represent the system of governing equations for the White-Metzner fluids. The viscosity η_1 is calculated by Eq. (2.14) and λ obeys Eq. (2.9). Viscosity η_2 is often taken as a function of η_1 . Note that the power-law constitutive equation can be obtained as a special case from Eq. (2.14).

2.3 Specialization to Axisymmetric Flows

The equations described in the preceding sections are valid for 2-D as well as 3-D flows and in any coordinate system (the equations are expressed in vector form). Here we specialize these equations to axisymmetric 2-D flows. The following vector representations allow us to write the governing equations in the cylindrical coordinates:

$$\begin{aligned}
\underline{\nabla} &= \hat{e}_r \frac{\partial}{\partial r} + \hat{e}_\theta \frac{1}{r} \frac{\partial}{\partial \theta} + \hat{e}_z \frac{\partial}{\partial z} \\
\underline{u} &= u_r \hat{e}_r + u_\theta \hat{e}_\theta + u_z \hat{e}_z = u \hat{e}_r + w \hat{e}_z \\
\underline{\tau} &= \tau_{rr} \hat{e}_r \hat{e}_{rr} + \tau_{\theta\theta} \hat{e}_\theta \hat{e}_\theta + \tau_{zz} \hat{e}_z \hat{e}_z \\
&\quad + \tau_{rz} (\hat{e}_r \hat{e}_z + \hat{e}_z \hat{e}_r) + \dots \\
\frac{\partial \hat{e}_r}{\partial \theta} &= \hat{e}_\theta, \quad \frac{\partial \hat{e}_\theta}{\partial \theta} = -\hat{e}_r
\end{aligned} \tag{2.15}$$

where $(\hat{e}_r, \hat{e}_\theta, \hat{e}_z)$ are the unit base vectors. For axisymmetric flows, all components of velocity and stresses are assumed to be independent of the angular coordinate θ , and depend only on the radial coordinate r and the z -coordinate. In summary, the governing equations (2.2), (2.13) and (2.14) become

$$\frac{\partial u}{\partial r} + \frac{u}{r} + \frac{\partial w}{\partial z} = 0 \tag{2.16}$$

$$\begin{aligned}
\frac{\partial}{\partial r} (\tau_{rr} + 2\eta_2 \frac{\partial u}{\partial r}) + \frac{1}{r} (\tau_{rr} + 2\eta_2 \frac{\partial u}{\partial r} - \tau_{\theta\theta} - 2\eta_2 \frac{u}{r}) \\
+ \frac{\partial}{\partial z} [\tau_{rz} + \eta_2 (\frac{\partial u}{\partial z} + \frac{\partial w}{\partial r})] - \frac{\partial P}{\partial r} = \rho [(\frac{\partial u}{\partial t} + u \frac{\partial u}{\partial r} + w \frac{\partial u}{\partial z})] \\
\frac{\partial}{\partial r} [\tau_{rz} + \eta_2 (\frac{\partial u}{\partial z} + \frac{\partial w}{\partial r})] + \frac{1}{r} [\tau_{rz} + \eta_2 (\frac{\partial u}{\partial z} + \frac{\partial w}{\partial r})] \\
+ \frac{\partial}{\partial z} (\tau_{zz} + 2\eta_2 \frac{\partial w}{\partial z}) - \frac{\partial P}{\partial z} = \rho (\frac{\partial w}{\partial t} + u \frac{\partial w}{\partial r} + w \frac{\partial w}{\partial z})
\end{aligned} \tag{2.17}$$

$$\tau_{rr} + \lambda \left[\frac{\partial \tau_{rr}}{\partial t} + u \frac{\partial \tau_{rr}}{\partial r} + w \frac{\partial \tau_{rr}}{\partial z} - 2 \left(\frac{\partial u}{\partial r} \tau_{rr} + \frac{\partial u}{\partial z} \tau_{rz} \right) \right] = 2\eta_1 \frac{\partial u}{\partial r}$$

$$\tau_{zz} + \lambda \left[\frac{\partial \tau_{zz}}{\partial t} + u \frac{\partial \tau_{zz}}{\partial r} + w \frac{\partial \tau_{zz}}{\partial z} - 2 \left(\frac{\partial w}{\partial z} \tau_{zz} + \frac{\partial w}{\partial r} \tau_{rz} \right) \right] = 2\eta_1 \frac{\partial w}{\partial z}$$

$$\begin{aligned} \tau_{rZ} + \lambda \left[\frac{\partial \tau_{rZ}}{\partial t} + u \frac{\partial \tau_{rZ}}{\partial r} + w \frac{\partial \tau_{rZ}}{\partial z} - 2 \left(\frac{\partial u}{\partial r} \tau_{rZ} + \frac{\partial w}{\partial z} \tau_{rZ} + \frac{\partial u}{\partial z} \tau_{ZZ} + \frac{\partial w}{\partial r} \tau_{rr} \right) \right] \\ = \eta_1 \left(\frac{\partial w}{\partial r} + \frac{\partial u}{\partial z} \right) \end{aligned}$$

$$\tau_{\theta\theta} + \lambda \left[\frac{\partial \tau_{\theta\theta}}{\partial t} + u \frac{\partial \tau_{\theta\theta}}{\partial r} + w \frac{\partial \tau_{\theta\theta}}{\partial z} - 2 \frac{u}{r} \tau_{\theta\theta} \right] = 2\eta_1 \frac{u}{r} \quad (2.18)$$

The use of the penalty function method, in the end, amounts to replacing the pressure P by the expression,

$$P = -\gamma_p (\underline{\nabla} \cdot \underline{u}) \quad (2.19)$$

where γ_p denotes the penalty parameter (preselected). For details, see [17, 20-22].

CHAPTER III
FINITE ELEMENT MODEL

3.1 The Penalty Function Formulation

The penalty function method is an approximate technique of including constraints into variational formulations. The penalty function method transforms a given constrained variational problem into an (actually, a sequence of) unconstrained variational problem(s) by the introduction of a penalty on the infringement of constraints [17,43]. Equations (2.1) and (2.3) subject to the constraint in equation (2.2). The point of view enables us to employ the penalty function method to formulate the problem variationally, and subsequently by the finite element method.

Over a typical element, the variational form of Eqns. (2.13) and (2.14) is given by

$$0 = \int_{\Omega^e} \left\{ \rho [\delta \underline{u} \cdot \frac{\partial \underline{u}}{\partial t} + \delta \underline{u} \cdot (\underline{u} \cdot \nabla \underline{u})] + \gamma_p \nabla \cdot (\delta \underline{u}) \nabla \cdot \underline{u} + \nabla (\delta \underline{u}) : (\underline{\tau} + 2\eta_2 \dot{\underline{y}}) \right\} dA - \int_{\Gamma^e} \delta \underline{u} \cdot \underline{t} ds \quad (3.1)$$

$$0 = \int_{\Omega^e} \left\{ \delta \underline{\tau} : \underline{\tau} + \lambda [\delta \underline{\tau} : \frac{\partial \underline{\tau}}{\partial t} + \delta \underline{\tau} : (\underline{u} \cdot \nabla \underline{\tau}) - \delta \underline{\tau} : ((\nabla \underline{u})^t \cdot \underline{\tau}) - \delta \underline{\tau} : (\underline{\tau} \cdot (\nabla \underline{u}))] - 2\eta_1 \delta \underline{\tau} : \dot{\underline{y}} \right\} dA \quad (3.2)$$

where δ denotes the variational symbol,

$$\underline{t} = (\underline{n} \cdot \underline{\tau})^t - \underline{n}P + \eta_2 (\underline{n} \cdot \underline{y})^t$$

and $\underline{\tau} : \underline{\tau}$ denotes the 'double-dot product', $\tau_{ij}\tau_{ji}$.

3.1.1 Plane Flow

Let u and v be the velocity components in the x and y directions respectively, and τ_{xx} , τ_{yy} and τ_{xy} be the extra stress components. Equations (2.17) and (2.18) can now be explicitly written for plane unsteady flows as follows:

$$\begin{aligned}
 0 = \int_{\Omega^e} \{ & \rho [\delta u \frac{\partial u}{\partial t} + \delta v \frac{\partial v}{\partial t} + \delta u (u \frac{\partial u}{\partial x} + v \frac{\partial u}{\partial y}) + \delta v (u \frac{\partial v}{\partial x} + v \frac{\partial v}{\partial y})] \\
 & + \gamma_P (\frac{\partial \delta u}{\partial x} + \frac{\partial \delta v}{\partial y}) (\frac{\partial u}{\partial x} + \frac{\partial v}{\partial y}) + \frac{\partial \delta u}{\partial x} (\tau_{xx} + 2\eta_2 \frac{\partial u}{\partial x}) \\
 & + \frac{\partial \delta u}{\partial y} [\tau_{xy} + \eta_2 (\frac{\partial u}{\partial y} + \frac{\partial v}{\partial x})] + \frac{\partial \delta v}{\partial x} [\tau_{xy} + \eta_2 (\frac{\partial u}{\partial y} + \frac{\partial v}{\partial x})] \\
 & + \frac{\partial \delta v}{\partial y} (\tau_{yy} + 2\eta_2 \frac{\partial v}{\partial y}) \} dx dy - \int_{\Gamma^e} (\delta u t_x + \delta v t_y) ds \quad (3.3)
 \end{aligned}$$

$$\begin{aligned}
 0 = \int_{\Omega^e} \{ & \delta \tau_{xx} \tau_{xx} + 2\delta \tau_{xy} \tau_{xy} + \delta \tau_{yy} \tau_{yy} + \lambda [\delta \tau_{xx} \frac{\partial \tau_{xx}}{\partial t} + 2\delta \tau_{xy} \frac{\partial \tau_{xy}}{\partial t} \\
 & + \delta \tau_{yy} \frac{\partial \tau_{yy}}{\partial t} + \delta \tau_{xx} (u \frac{\partial \tau_{xx}}{\partial x} + v \frac{\partial \tau_{xx}}{\partial y}) + 2\delta \tau_{xy} (u \frac{\partial \tau_{xy}}{\partial x} + v \frac{\partial \tau_{xy}}{\partial y}) \\
 & + \delta \tau_{yy} (u \frac{\partial \tau_{yy}}{\partial x} + v \frac{\partial \tau_{yy}}{\partial y}) - \delta \tau_{xx} (\frac{\partial u}{\partial x} \tau_{xx} + \frac{\partial u}{\partial y} \tau_{xy}) \\
 & - \delta \tau_{xy} (\frac{\partial v}{\partial x} \tau_{xx} + \frac{\partial v}{\partial y} \tau_{xy}) - \delta \tau_{xy} (\frac{\partial u}{\partial x} \tau_{xy} + \frac{\partial u}{\partial y} \tau_{yy}) \\
 & - \delta \tau_{yy} (\frac{\partial v}{\partial x} \tau_{xy} + \frac{\partial v}{\partial y} \tau_{yy}) - \delta \tau_{xx} (\tau_{xx} \frac{\partial u}{\partial x} + \tau_{xy} \frac{\partial u}{\partial y}) \\
 & - \delta \tau_{xy} (\tau_{xy} \frac{\partial u}{\partial x} + \tau_{yy} \frac{\partial u}{\partial y}) - \delta \tau_{xy} (\tau_{xx} \frac{\partial v}{\partial x} + \tau_{xy} \frac{\partial v}{\partial y})
 \end{aligned}$$

$$\begin{aligned}
& - \delta\tau_{yy}(\tau_{xy} \frac{\partial v}{\partial x} + \tau_{yy} \frac{\partial v}{\partial y})] - 2\eta_1[\delta\tau_{xx} \frac{\partial u}{\partial x} + \delta\tau_{yy} \frac{\partial v}{\partial y} \\
& + \delta\tau_{xy}(\frac{\partial u}{\partial y} + \frac{\partial v}{\partial x})] \} dx dy \quad (3.4)
\end{aligned}$$

3.1.2 Axisymmetric Flow

In cylindrical coordinates let u and w be the velocity components in the radial and axial directions respectively, and τ_{rr} , τ_{rz} , τ_{zz} and $\tau_{\theta\theta}$ be the extra stress components. For axisymmetric flow, the stress component $\tau_{\theta\theta}$ appears explicitly in the momentum equation and it is necessary to add an explicit constitutive equation for obtaining $\tau_{\theta\theta}$. Thus the system consists of six dependent unknowns. Equation (2.17) and Eq. (2.18) can be written for axisymmetric unsteady flows as follows:

$$\begin{aligned}
0 = \int_{\Omega^e} \{ & \rho[\delta u \frac{\partial u}{\partial t} + \delta w \frac{\partial w}{\partial t} + \delta u(u \frac{\partial u}{\partial r} + w \frac{\partial u}{\partial z}) + \delta w(u \frac{\partial w}{\partial r} + w \frac{\partial w}{\partial z})] \\
& + \gamma_p (\frac{\partial \delta u}{\partial r} + \frac{1}{r} \delta u + \frac{\partial \delta w}{\partial z})(\frac{u}{r} + \frac{\partial u}{\partial r} + \frac{\partial w}{\partial z}) \\
& + \frac{\partial \delta u}{\partial r} [\tau_{rr} + 2\eta_2 \frac{\partial u}{\partial r}] + \frac{\partial \delta u}{\partial z} [\tau_{zr} + \eta_2(\frac{\partial u}{\partial z} + \frac{\partial w}{\partial r})] \\
& + \frac{\partial \delta w}{\partial r} [\tau_{zr} + \eta_2(\frac{\partial u}{\partial z} + \frac{\partial w}{\partial r})] + \frac{1}{r} \delta u(\tau_{\theta\theta} + 2\eta_2 \frac{u}{r}) \\
& + \frac{\partial \delta w}{\partial z} (\tau_{zz} + 2\eta_2 \frac{\partial w}{\partial z}) \} r dr dz \\
& - \int_{\Gamma^e} (\delta u t_r + \delta w t_z) ds \quad (3.5)
\end{aligned}$$

$$0 = \int_{\Omega^e} \{ \delta\tau_{rr}\tau_{rr} + \delta\tau_{\theta\theta}\tau_{\theta\theta} + 2\delta\tau_{rz}\tau_{rz} + \delta\tau_{zz}\tau_{zz}$$

$$\begin{aligned}
& + \lambda [\delta\tau_{rr} \frac{\partial\tau_{rr}}{\partial t} + \delta\tau_{\theta\theta} \frac{\partial\tau_{\theta\theta}}{\partial t} + 2\delta\tau_{rz} \frac{\partial\tau_{rz}}{\partial t} + \delta\tau_{zz} \frac{\partial\tau_{zz}}{\partial t} \\
& + \delta\tau_{rr} (u \frac{\partial\tau_{rr}}{\partial r} + w \frac{\partial\tau_{rr}}{\partial z}) + \delta\tau_{\theta\theta} (u \frac{\partial\tau_{\theta\theta}}{\partial r} + w \frac{\partial\tau_{\theta\theta}}{\partial z}) \\
& + \delta\tau_{zz} (u \frac{\partial\tau_{zz}}{\partial r} + w \frac{\partial\tau_{zz}}{\partial z}) + 2\delta\tau_{rz} (u \frac{\partial\tau_{rz}}{\partial r} + w \frac{\partial\tau_{rz}}{\partial z}) \\
& - 2\delta\tau_{rr} (\frac{\partial u}{\partial r} \tau_{rr} + \frac{\partial u}{\partial z} \tau_{rz}) - 2\delta\tau_{\theta\theta} \frac{u}{r} \tau_{\theta\theta} \\
& - 2\delta\tau_{zz} (\frac{\partial w}{\partial z} \tau_{zz} + \frac{\partial w}{\partial r} \tau_{rz}) - 2\delta\tau_{rz} (\frac{\partial u}{\partial r} \tau_{rz} + \frac{\partial u}{\partial z} \tau_{zz} + \frac{\partial w}{\partial z} \tau_{rz} + \frac{\partial w}{\partial r} \tau_{rr}) \\
& - 2\eta_1 [\delta\tau_{rr} \frac{\partial u}{\partial r} + \delta\tau_{\theta\theta} \frac{u}{r} + \delta\tau_{zz} \frac{\partial w}{\partial z} + \delta\tau_{rz} (\frac{\partial w}{\partial r} + \frac{\partial u}{\partial z})] \} r dr dz \quad (3.6)
\end{aligned}$$

3.2 Finite Element Models

3.2.1 Plane Flow

The velocities and the extra stress components can be interpolated over an element by following expressions (see Reddy [17,43])

$$\begin{aligned}
u(x,y,t) &= \sum_{j=1}^N u_j(t) \psi_j(x,y) \\
v(x,y,t) &= \sum_{j=1}^N v_j(t) \psi_j(x,y) \\
\tau_{xx}(x,y,t) &= \sum_{j=1}^L \tau_{xx}^j(t) \psi_j(x,y) \\
\tau_{yy}(x,y,t) &= \sum_{j=1}^L \tau_{yy}^j(t) \psi_j(x,y) \\
\tau_{xy}(x,y,t) &= \sum_{j=1}^L \tau_{xy}^j(t) \psi_j(x,y) \quad (3.7)
\end{aligned}$$

where u_j , v_j are the velocities and τ_{xx}^j , τ_{yy}^j , τ_{xy}^j are the extra stress components at the nodal points, and ψ_j are the interpolation functions (see [17,43]).

The shape functions used for extra stress components are identical to those used for the velocity components. A detailed discussion is given by Crochet, Davies and Walters [38]. In general, there are five degrees of freedom per node.

Substitution of Eq. (3.7) into Eqs. (3.3) and (3.4), we obtain

$$[M^e]\{\dot{\Delta}^e\} + [K^e]\{\Delta^e\} = \{F^e\} \quad (3.8)$$

where

$$\{\Delta\} = \begin{pmatrix} \{u\} \\ \{v\} \\ \{\tau_{xx}\} \\ \{\tau_{yy}\} \\ \{\tau_{xy}\} \end{pmatrix} \quad (3.9)$$

is a solution vector, $\{F\}$ is the force vector and $[M]$ and $[K]$ are the mass and coefficient matrices (see Appendix A).

For steady plane flow, $\{\dot{\Delta}^e\}$ will be zero and the element equation (3.8) takes the form,

$$[K^e]\{\Delta^e\} = \{F^e\} \quad (3.10)$$

For unsteady flows, an approximation of time derivatives must be used. We shall return to time approximations later.

3.2.2 Axisymmetric Flow

The velocities and extra stress component can be interpolated over an element by the following expressions

$$\begin{aligned}
 u(r,z,t) &= \sum_{j=1}^N u_j(t) \psi_j(r,z) \\
 w(r,z,t) &= \sum_{j=1}^N w_j(t) \psi_j(r,z) \\
 \tau_{rr}(r,z,t) &= \sum_{j=1}^L \tau_{rr}^j(t) \psi_j(r,z) \\
 \tau_{zz}(r,z,t) &= \sum_{j=1}^L \tau_{zz}^j(t) \psi_j(r,z) \\
 \tau_{rz}(r,z,t) &= \sum_{j=1}^L \tau_{rz}^j(t) \psi_j(r,z) \\
 \tau_{\theta\theta}(r,z,t) &= \sum_{j=1}^L \tau_{\theta\theta}^j(t) \psi_j(r,z)
 \end{aligned} \tag{3.11}$$

where (u_j, w_j) are the nodal velocities and $(\tau_{rr}^j, \tau_{zz}^j, \tau_{rz}^j, \tau_{\theta\theta}^j)$ are the nodal extra stress components.

Substituting Eq. (3.11), into Eq. (3.5) and (3.6), we obtain the element equations

$$[M^e] \{\dot{\Delta}^e\} + [K^e] \{\Delta^e\} = \{F^e\} \tag{3.12}$$

where

$$\{\Delta^e\} = \begin{pmatrix} \{u\} \\ \{w\} \\ \{\tau_{rr}\} \\ \{\tau_{zz}\} \\ \{\tau_{rz}\} \\ \{\tau_{\theta\theta}\} \end{pmatrix} \quad (3.13)$$

The coefficient matrices for axisymmetric flow are listed in Appendix B.

3.3 Boundary Conditions

For Newtonian fluids, it is sufficient to specify velocities as the essential boundary conditions. The mixed formulation of Newtonian fluids or power-law fluids allow the specification of velocities and stresses, but for such fluids only one or the other can be specified. In the penalty finite element method, the specification of pressure does not constitute an essential boundary condition. For viscoelastic fluids, specification of velocities is insufficient on account of fluid memory. If the boundary of the domain contains an entry region, then fully-developed flow conditions should be assumed. All the extra stress components must be specified as essential boundary conditions along the entry region. Failing to do so may lead to the propagation of errors throughout the flow domain when relaxation time λ becomes large.

There are three different types of boundaries in the flow problems that are studied here: inlet and outlet surfaces, wall boundaries and flow centerlines. For entry region, fully developed flow conditions are assumed. All the extra stress components are specified at the inlet.

For walls, the no slip condition is assumed, and at the centerline symmetry conditions are used.

3.4 Time Approximations

Equations (3.8) and (3.12) need further approximation to reduce the ordinary differential equations in time to algebraic equations. Here we use the alpha-family of approximation (see [17]). Consider Eq. (3.8), which is valid for any time $t > 0$. Suppose that the solution $\{\Delta\}$ is known at time $t = t_n \equiv (n + 1) \Delta t$, Δt being the time step and n is an integer. In the α -family of approximation, the time derivative $\{\dot{\Delta}\}$ at time t_{n+1} is approximated according to

$$\alpha \{\dot{\Delta}\}_{n+1} = \frac{1}{\Delta t} [\{\Delta\}_{n+1} - \{\Delta\}_n] - (1 - \alpha) \{\dot{\Delta}\}_n \quad (3.14)$$

Use of Eq. (3.14) in Eq. (3.8) yields the algebraic equations for an element

$$[\hat{K}]\{\Delta\}_{n+1} = \{\hat{F}\}_{n+1} \quad (3.15)$$

where

$$[\hat{K}] = [K(\Delta_n)] + \alpha \Delta t [M]$$

$$\{\hat{F}\}_{n+1} = ([K(\Delta_n)] - (1 - \alpha) \Delta t [M]) \{\Delta\}_n + (\alpha \{F\}_{n+1} + (1 - \alpha) \{F\}_n) \Delta t \quad (3.16)$$

The algebraic equations (3.15) are assembled in the usual manner to obtain the equations for the total problem.

3.5 Iterative Technique

Note that the assembled equations associated with (3.15) are nonlinear, requiring an iterative solution. At each iteration, all the nonlinear terms are evaluated using the solution from the previous iteration. Hence, at each iteration the system becomes linear and can be solved after imposing boundary conditions. The iteration continues until the difference between two successive iterative solutions is less than a specified value. The method described above is called 'picard iteration technique'. In order to accelerate the convergence of such technique, a weighted average of the last two iterative solutions is used to evaluate the nonlinear coefficients in the present iteration.

At $(r + 1)$ st iteration Eq. (3.15) reads as (see [17,43])

$$[\hat{K}(\bar{\Delta}_n)] \{\Delta^{r+1}\}_{n+1} = \{\hat{F}\}_{n+1} \quad (3.17)$$

where $\{\bar{\Delta}\}_n$ denotes the average

$$\{\bar{\Delta}\}_n = \beta \{\Delta^r\}_n + (1 - \beta) \{\Delta^{r+1}\}_n$$

and $\{\Delta^r\}_n$ is the solution at r -th iteration and time $t = t_n$.

Convergence criterion is given by

$$\sqrt{\frac{\sum_{i=1}^n |\Delta_i^{r+1} - \Delta_i^r|^2}{\sum_{i=1}^n |\Delta_i^{r+1}|^2}} < \epsilon \quad (3.18)$$

where ϵ is the tolerance (say 0.01).

CHAPTER IV

NUMERICAL RESULTS

4.1 Preliminary Comments

The finite element models presented in Chapter III are implemented in FORTRAN on an IBM 3090 Processor. All computations were carried out in double-precision arithmetics. Although the computer program developed contains both velocity and velocity-stress (i.e. mixed) models, most of the results presented here are obtained using the mixed model.

All of the numerical calculations concern plane or axisymmetric flows in two basic geometries: (i) uniform channel or tube, and (ii) four-to-one-contraction of channels or tubes. The general geometries and computational domains (utilized the symmetry) are shown in Figs. 1 and 2. The velocity boundary conditions are also indicated in the figure. The meshes used for the domains are shown in Figures 3 and 4.

4.2 Discussion of the Results

4.2.1 Effect of Mesh

First, the effect of mesh on the accuracy (i.e., numerical convergence) of the solution is investigated using the axisymmetric flow of a power-law fluid in a uniform tube ($R = 1$, $L = 6$, $w_0 = 10.0$, $n = 0.2$, $\eta_0 = 1.0$, $\eta_2 = 0$). Four different (uniform and nonuniform) meshes are used (see Fig. 3) in the study, and the results obtained are listed in Table 1. In this study the inertia effects are omitted, and the velocity model is used. Note that Meshes 1, 2 and 3 are increasingly finer meshes, and Meshes 1 and 2 are uniform and Mesh 3 is nonuniform.

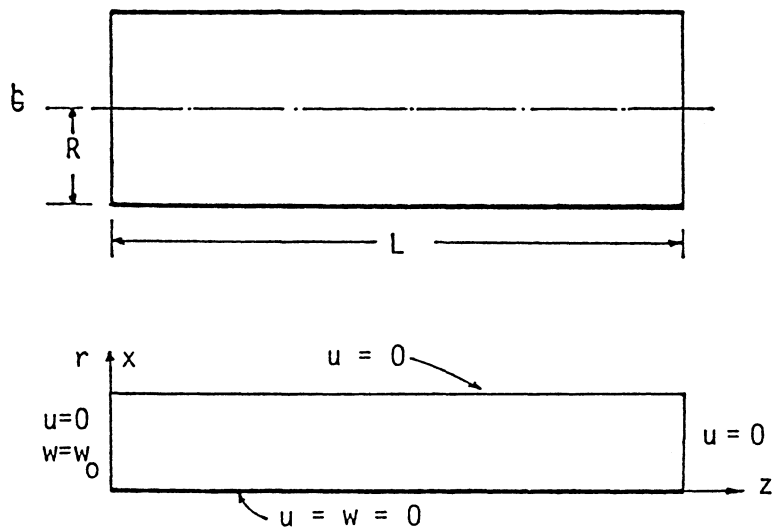


Figure 1. Geometry and computational domain with velocity boundary conditions for flow in a channel or pipe.

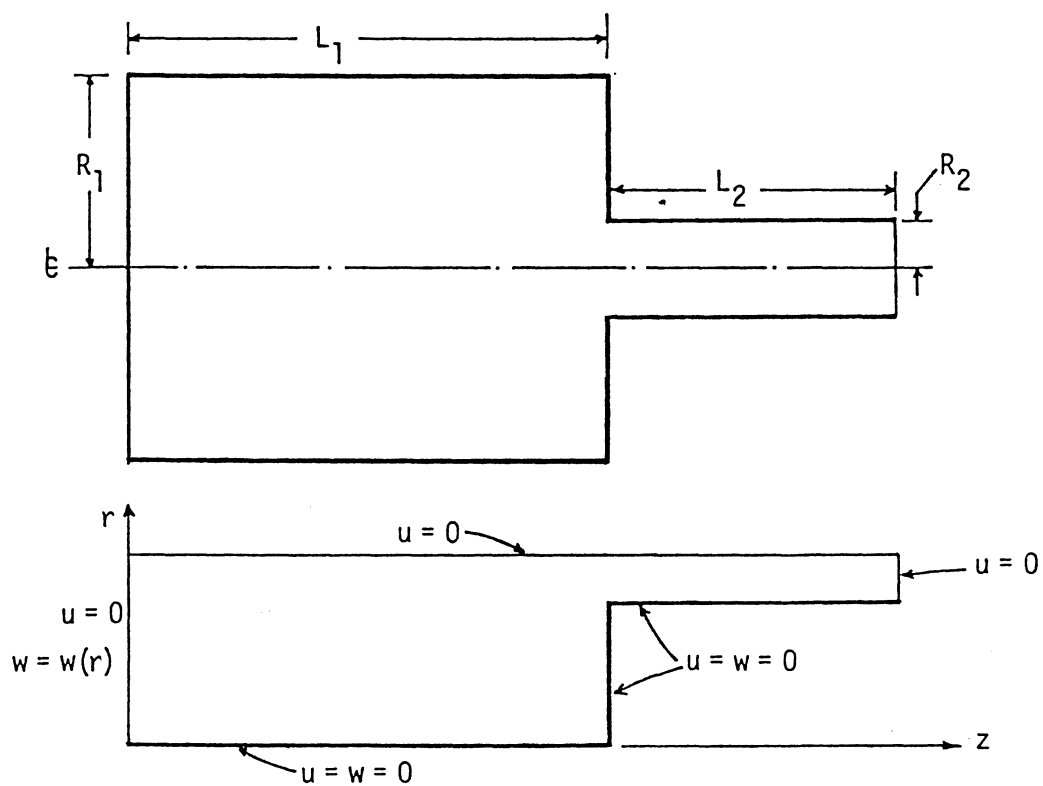
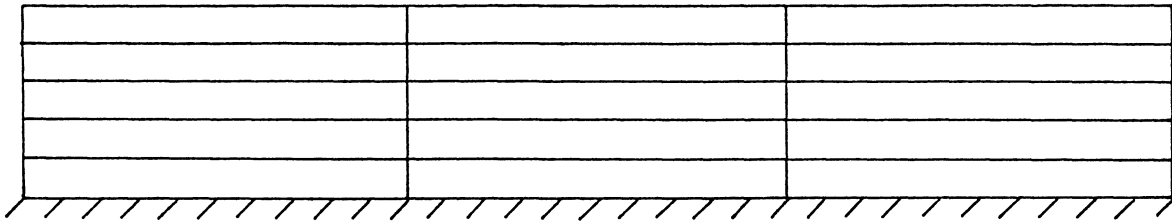
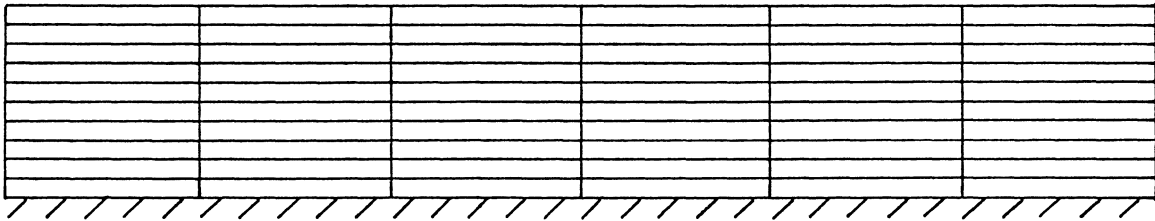


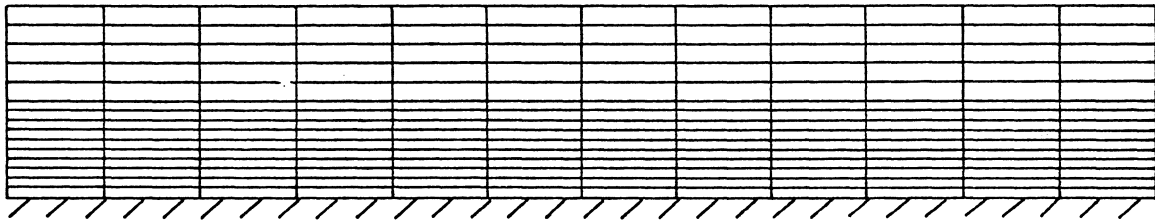
Figure 2. Geometry and computational domain with velocity boundary conditions for flow through a four-to-one (4:1) contraction channel or tube.



Mesh 1



Mesh 2



Mesh 3

Figure 3. The three finite element meshes used in the finite element analysis of power-law fluid in a pipe.

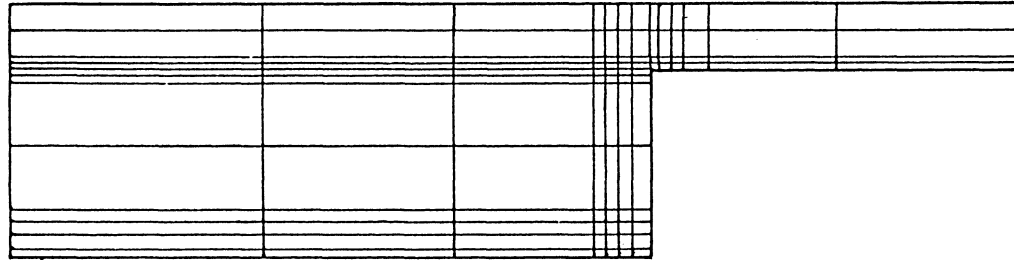


Figure 4. The nonuniform mesh of linear elements used for the contraction problem. ($L_1 = 10$, $L_2 = 6$, $R_1 = 4$ and $R_2 = 1$).

TABLE 1

Effect of mesh refinement on the velocity profile for the flow of power-law fluid ($n = 0.2$) in a tube ($w_0 = 10.0$, $\gamma_p = 10^8$)

Radial Distance r	Velocity, $w(r,6)$			Analytical
	Mesh 1	Mesh 2	Mesh 3	
0.00	11.894	12.833	13.402	13.333
0.05	-	-	-	13.333
0.10	-	12.832	13.401	13.333
0.15	-	-	-	13.333
0.20	11.865	12.826	13.395	13.332
0.25	-	-	-	13.330
0.30	-	12.795	13.360	13.324
0.35	-	-	-	13.309
0.40	11.721	12.686	13.243	13.279
0.45	-	-	-	13.223
0.50	-	12.401	12.940	13.125
0.55	-	-	12.679	12.964
0.60	10.852	11.783	12.305	12.711
0.65	-	-	11.787	12.328
0.70	-	10.610	11.086	11.765
0.75	-	-	10.156	10.960
0.80	7.916	8.563	8.946	9.838
0.85	-	-	7.396	8.305
0.90	-	5.133	5.451	6.248
0.95	-	-	2.993	3.532
1.00	0.000	0.000	0.000	0.000

Table 1 also contains the analytical solution of the fully developed flow. The convergence of the solution with refinement of the mesh is clear. Note that in the finite element method, it is not correct to compare the solution at the nodes, because the solution converges in a variational (i.e., integral) sense.

4.2.2 Effect of Stress Boundary Conditions

Next, the effect of stress boundary conditions in the mixed model on the velocity and stress fields is investigated using both the power law, ($n = 0.25$, $\eta_0 = 10^3$, $\eta_2 = 0$) model and White-Metzner model ($n = 0.25$, $\eta_0 = 10^3$, $\eta_2 = 0$, $a = 0.435$, $b = -0.453$, $c = 0.1388$) for flow in a tube ($R = 1$ and $L = 5$). A uniform mesh 10×6 of linear elements is used. In addition to the velocity boundary conditions shown in Fig. 1, the stresses τ_{rr} , τ_{rz} , τ_{zz} and $\tau_{\theta\theta}$ are specified to be zero at the entrance. Figures 5 and 6 contain plots of axial velocity profiles at $z = 2.0$ and $z = 6.0$ obtained by specifying and not specifying the stress boundary conditions in the velocity and mixed finite element models. First, note that the velocity fields obtained using the velocity and mixed models, for power law fluids, without stress boundary conditions, are essentially the same. The stress boundary conditions (of course, applies only to the mixed model) do have effect on the velocity profile for power-law fluids; specification of stresses to be zero at the inlet of the tube increases the centerline velocity. Similar observation can be made for the White-Metzner fluid. Interestingly enough, if the stresses are not specified, numerical convergence of the nonlinear solution is not achieved for the White-Metzner fluids. This indicates

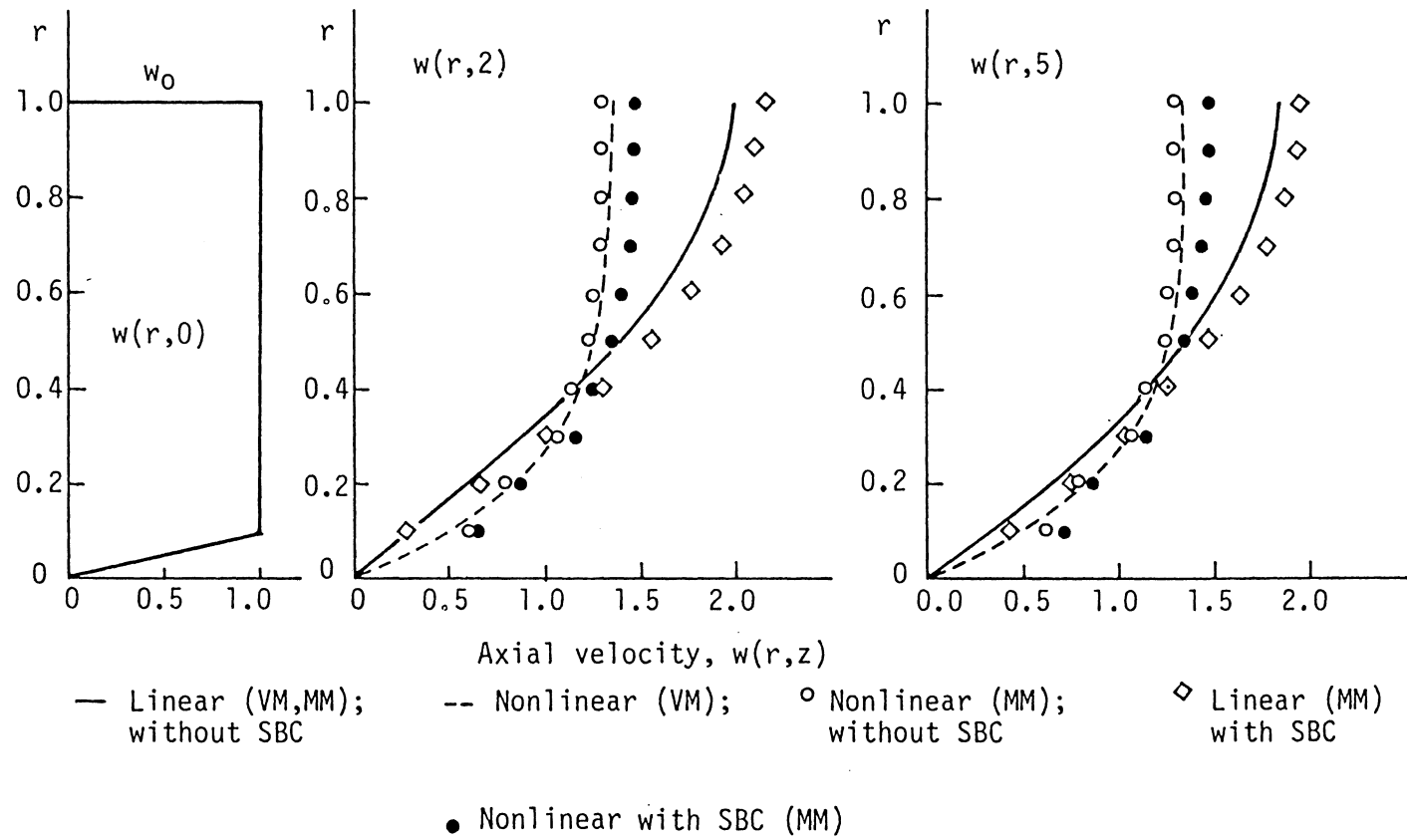


Figure 5. Comparison of the axial velocity profiles for the flow of a power-law fluid through a tube ($R=1$, $L=5$, $n=0.25$, $w_0=1$, $\eta_0=10^3$, $\eta_2=0$); VM = Velocity Model, MM = Mixed Model, SBC = Stress Boundary Conditions.

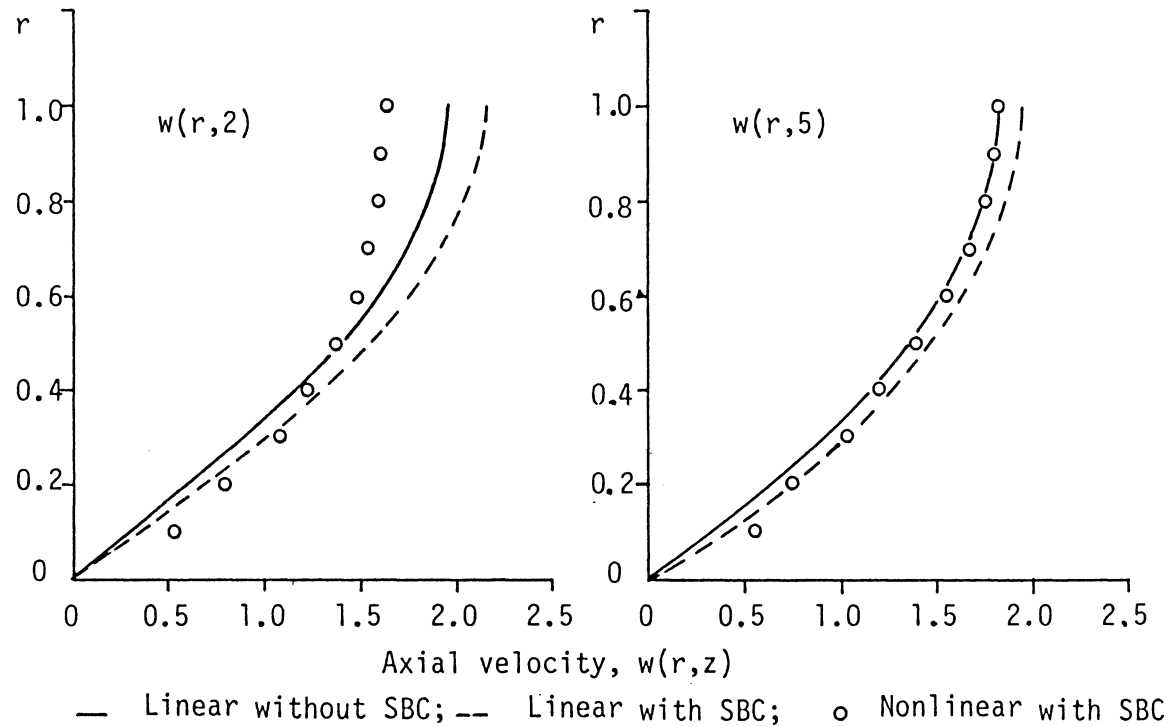


Figure 6. Comparison of the axial velocity profiles for the flow of the White-Metzner Fluid through a tube ($R=1$, $L=5$, $n=0.25$, $w_0=1$, $\eta_0=10^3$, $\eta_2=0$) for the mixed model (SBC=Stress Boundary Conditions)

that it is necessary to specify extra stress components at appropriate boundary points.

4.2.3 Effect of Inertia

The effect of inertia (i.e., convective) terms on the velocity field is investigated using the velocity model, and the results are presented in Table 2. The flow of a power-law fluid ($n = 0.25$, $\eta_0 = 10^3$, $\eta_2 = 0$) in a tube ($R = 1.0$, $L = 5.0$, $w_0 = 1.0$) is used in the study. From the results presented in Table 2, it is clear that the effect of inertia terms is to further 'flatten' the parabolic profile (in addition to that caused by the power-law constitutive model). This is expected because an increase in the Reynolds number is accompanied by a reduction of the boundary layer thickness near the wall.

4.2.4 Effect of Penalty Parameter

The effect of the value of the penalty parameter on the solution accuracy is also investigated for a power-law fluid ($n = 0.2$, $\eta_0 = 1.0$, $\eta_2 = 0$) in a tube ($R = 1.0$, $L = 6.0$, $w_0 = 12.5$). Figure 7 contains plots of axial velocity profiles at the exit for various values of the penalty parameter, γ_p . It is clear that values of γ_p between 10^4 to 10^{12} essentially give the same velocity profiles of Newtonian fluids. For γ_p less than 10^4 the accuracy of the solution deteriorates rapidly. On the other hand, for γ_p very large (say 10^{16}), the penalty terms outweigh the viscous terms and the resulting coefficient matrix becomes singular. For the power-law fluids (i.e., materially nonlinear analysis), it is interesting to note that the penalty parameter is less sensitive to the accuracy of the velocity field. Even for $\gamma_p = 10^2$, the

TABLE 2

Effect of the convective terms on the velocity field of a power-law fluid ($n = 0.2$, $\eta_0 = 10^3$, $\eta_2 = 0$) in a tube ($R = 1$, $L = 5$, 10×6 mesh of linear elements)

Radial Distance r	Velocity, $w(r,5)$			
	Newtonian	Re = 0.0		Re = 1000
		Non-Newtonian	Non-Newtonian	Non-Newtonian
			with inertia	with inertia
0.0	1.8358	1.3357	1.1312	1.0267
0.1	1.8001	1.3355	1.1302	1.0265
0.2	1.7398	1.3338	1.1289	1.0266
0.3	1.6461	1.3271	1.1270	1.0268
0.4	1.5186	1.3081	1.1241	1.0271
0.5	1.3578	1.2657	1.1197	1.0275
0.6	1.1651	1.1849	1.1097	1.0274
0.7	0.9397	1.0468	1.0799	1.0265
0.8	0.6712	0.8273	0.9809	1.0209
0.9	0.3079	0.4795	0.6709	0.8967
1.0	0.0000	0.0000	0.0000	0.0000

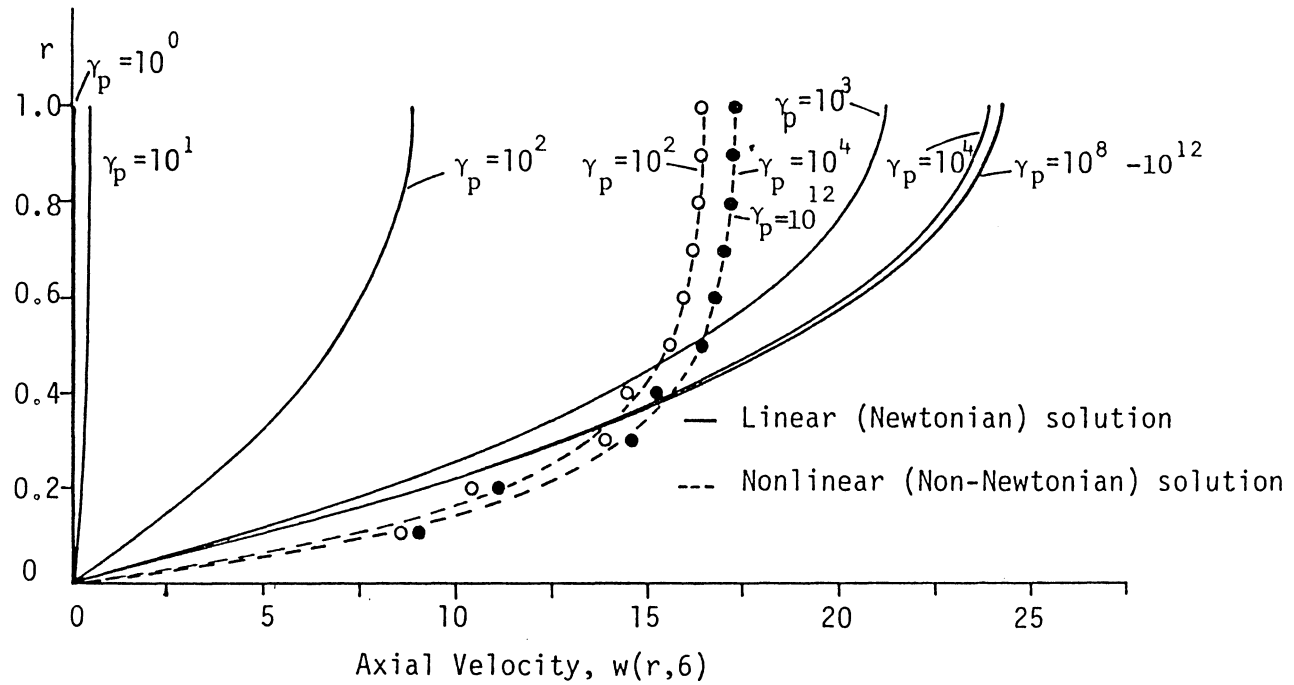


Figure 7. The effect of the penalty parameter on the linear and nonlinear axial velocity of the power-law fluid in a pipe ($R=1$, $L=6$, $n=0.2$, $\eta_0=1$, $\eta_2=0$); Mesh: 10×6 of linear elements; Stress boundary conditions at the entrance are imposed.

non-Newtonian solution is very close to that obtained using $\gamma_p = 10^4$ to 10^{12} .

4.2.5 Analysis of Power-Law Fluids

Consider the flow through a plane channel ($R = 1$, $L = 6$). The geometry and the boundary conditions of the problem are shown in Figure 1. A comparison study of the velocity profiles of Newtonian and power-law fluids with power index $n = 0.2$ ($\eta_0 = 1$, $\eta_2 = \eta_1$) is carried out. Inertial effect on the solution is also examined. The solutions are presented in Figure 8. The results for Newtonian case and power-law fluid without inertia are in very good agreement with the results published by Crochet, Davies and Walters [38]. For the Newtonian case, the velocity profile at the exit becomes parabolic which is initially flat. Here the viscous effects dominate the solution and make fluid to flow smoothly through the channel giving a parabolic profile at the exit. For the power-law fluid, viscous effects become less dominant. Thus, the fully developed profile becomes flatter. A comparison of velocity profiles for the power-law fluid without and with inertia are also shown in Figure 8. It is evident that the presence of inertia terms in the equation of motion dominate the viscous terms. The fluid tries to remain close to the wall and gives the flattest velocity profiles at the exit. Figure 9 shows the comparison between the pressure profiles without and with inertial effects. Both the profiles are smooth except at the wall. At the wall both the velocity components are zero and pressure becomes infinite and shows more fluctuations near the wall. Due to inertia, the pressure at the exit increases in value.

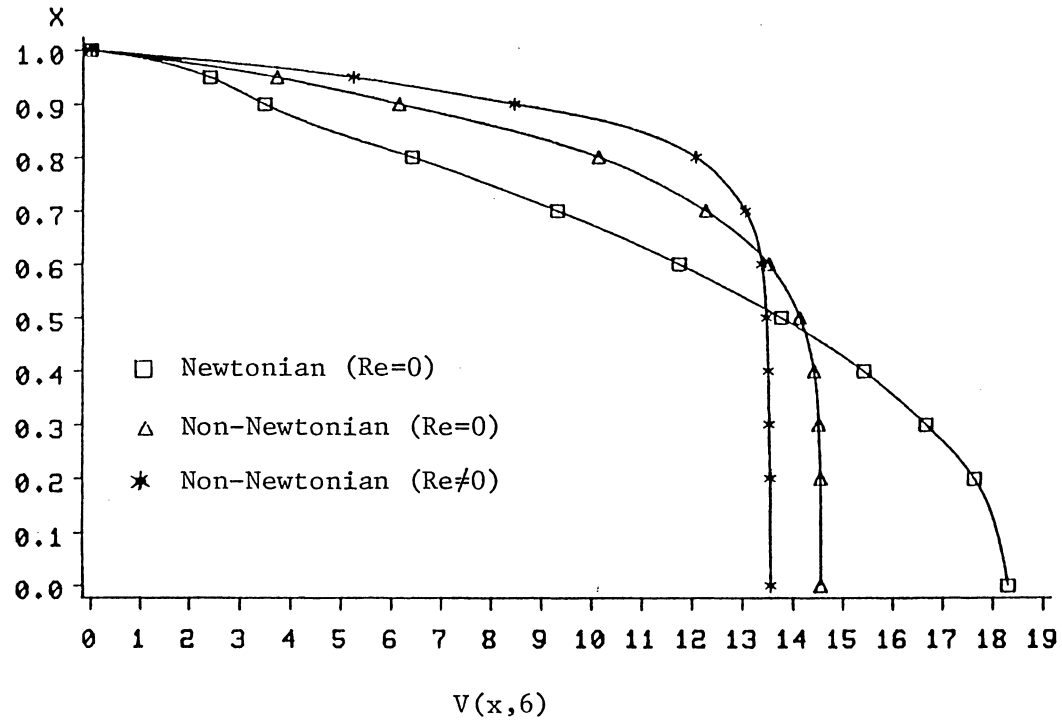


Figure 8. Velocity profiles for a power-law fluid in a plane channel ($V_0 = 12.5$, $n=0.2$, $\eta_2 = \eta_1$, $\eta_0 = 1.0$)

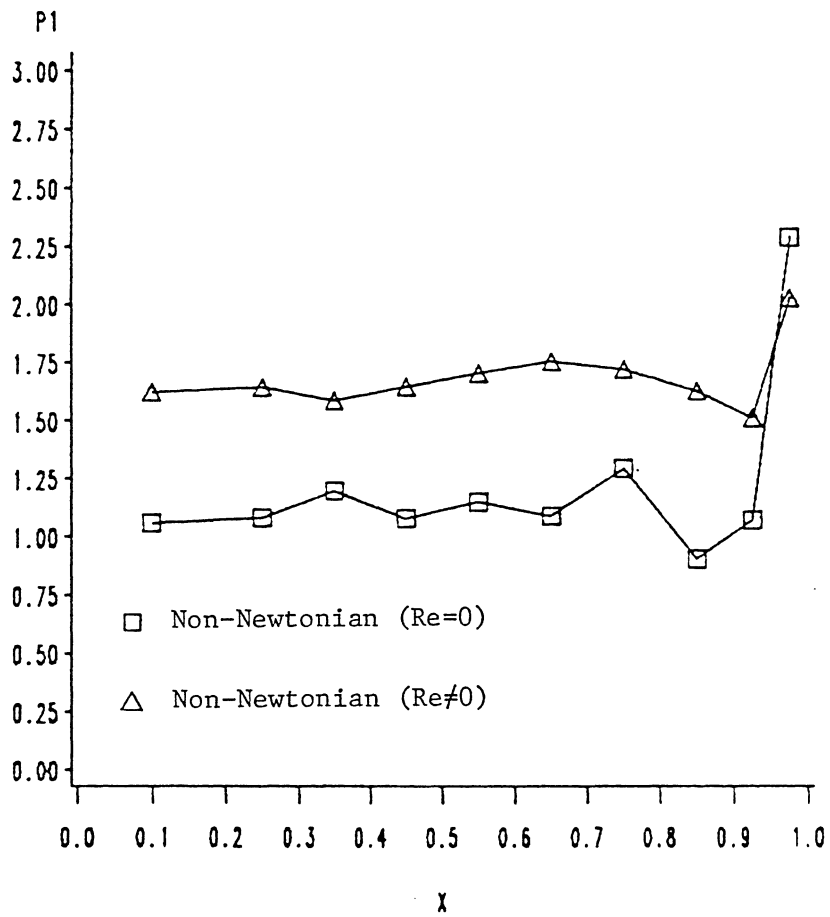


Figure 9. Pressure profiles for a power-law fluid in a plane channel ($V_0 = 12.5$)

The effects of inertia become more evident when the flow rate is increased (i.e. at higher Reynolds number, $Re = \rho R w_0 / \eta_0$). Figure 10 contains the velocity profiles of the Newtonian and power-law fluids for twice the velocity used before. Comparing Figure 10 with Figure 8, it can be clearly seen that the inertial effects become more dominant at the higher inlet velocity, and the velocity profile gets increasingly flatter. The pressure profiles, (see Figure 11) are similar to those in Figure 9, and show more fluctuation near the wall.

Next, the same power-law fluid is analyzed for flow through a tube ($R = 1, L = 6$). The results obtained are presented in Figures 12 through 15. The results obtained for the axisymmetric flow are very similar to the results obtained for the plane flow discussed earlier. Figure 12 contains velocity profiles of Newtonian fluid and power-law fluid with and without inertia. In Figure 13, a comparison of the pressure profiles with and without inertia is presented. Figure 14 and 15 contains results for higher flow rate. The observations made for the plane flow also hold for the axisymmetric flow and the velocity profiles obtained here are 98.5% of the fully developed flow and thus the accuracy of the model is verified. In Figure 16, the exit velocity profiles of the Newtonian fluid along with the power law fluid of $n = -0.6$ with and without inertia terms are presented. Newtonian fluid shows a fully developed velocity profile at the exit while for the power law fluid, a fully developed profile lends to a plug-flow (see [38]). From Figure 16 it is seen that at this high power index, the inertial effects do not affect the velocity profiles at all. The increased flow

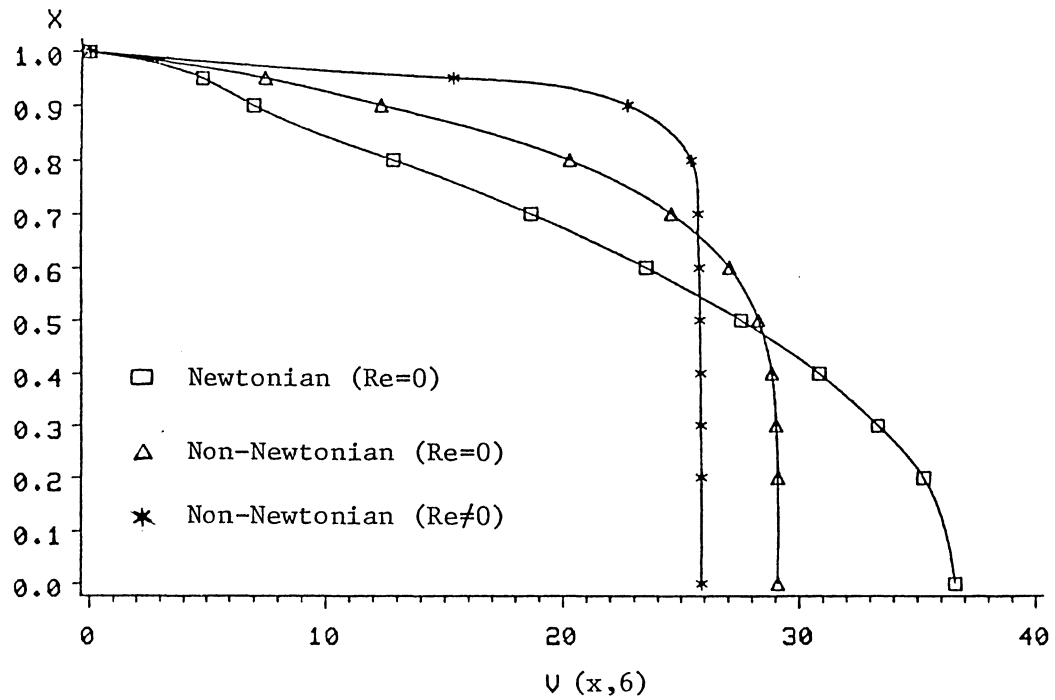


Figure 10. Velocity profiles for a power-law fluid in a plane channel ($V_0 = 25.0$, $n=0.2$, $\eta_2 = \eta_1$, $\eta_0=1.0$)

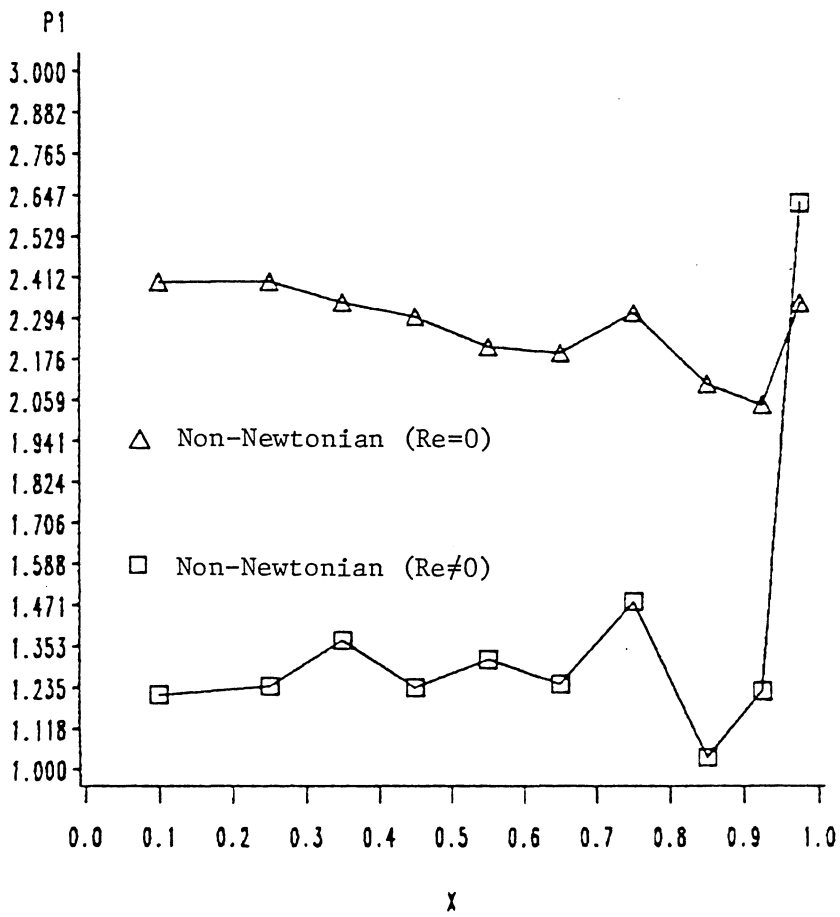


Figure 11. Pressure profiles for a power-law fluid in a channel ($V_0=25.0$)

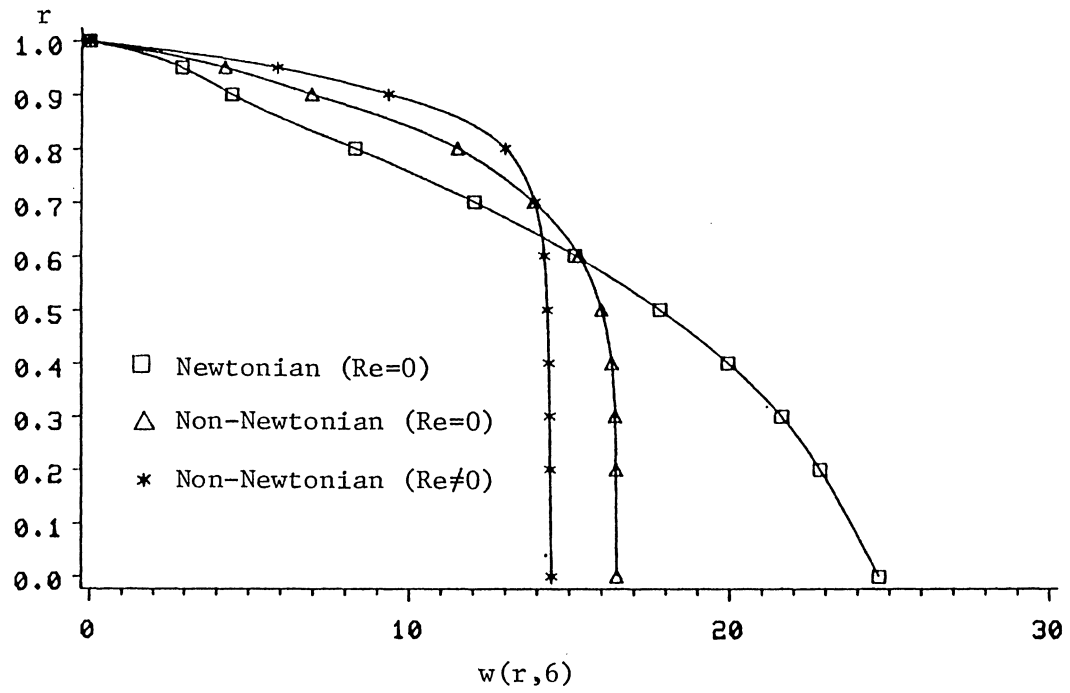


Figure 12. Velocity profiles for the power-law fluid through a pipe ($R=1.0$, $L=6.0$, $n=0.2$, $\eta_0=1.0$, $\eta_2=\eta_1$, $w_0=12.5$)

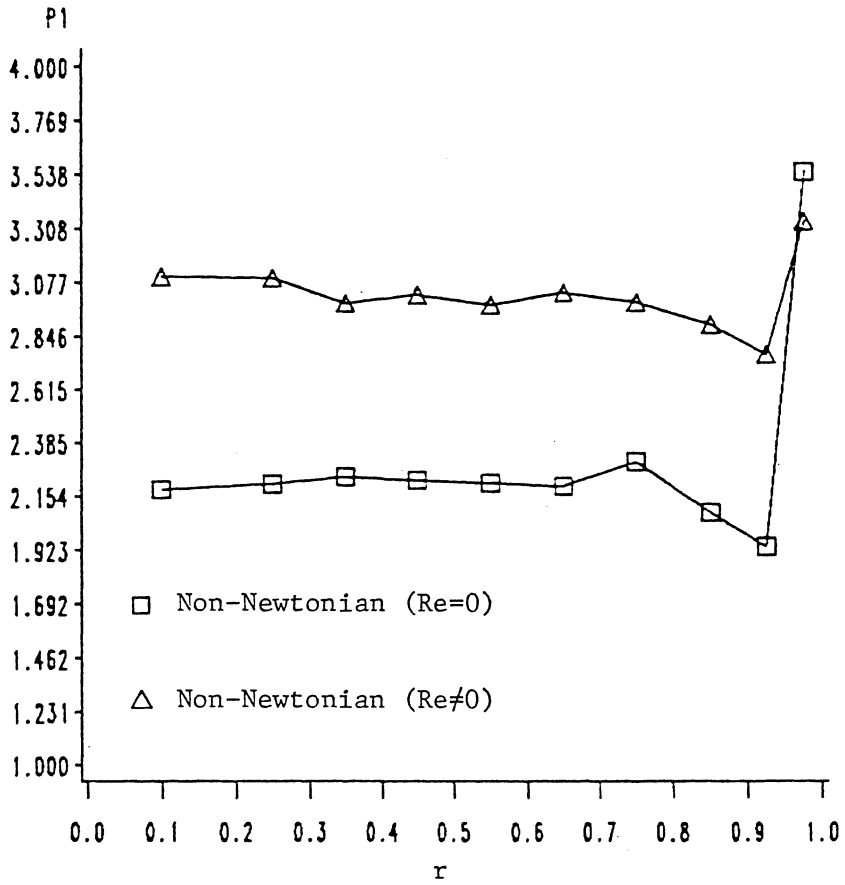


Figure 13. Pressure profiles for a power-law fluid through a pipe ($w_0=12.5$)

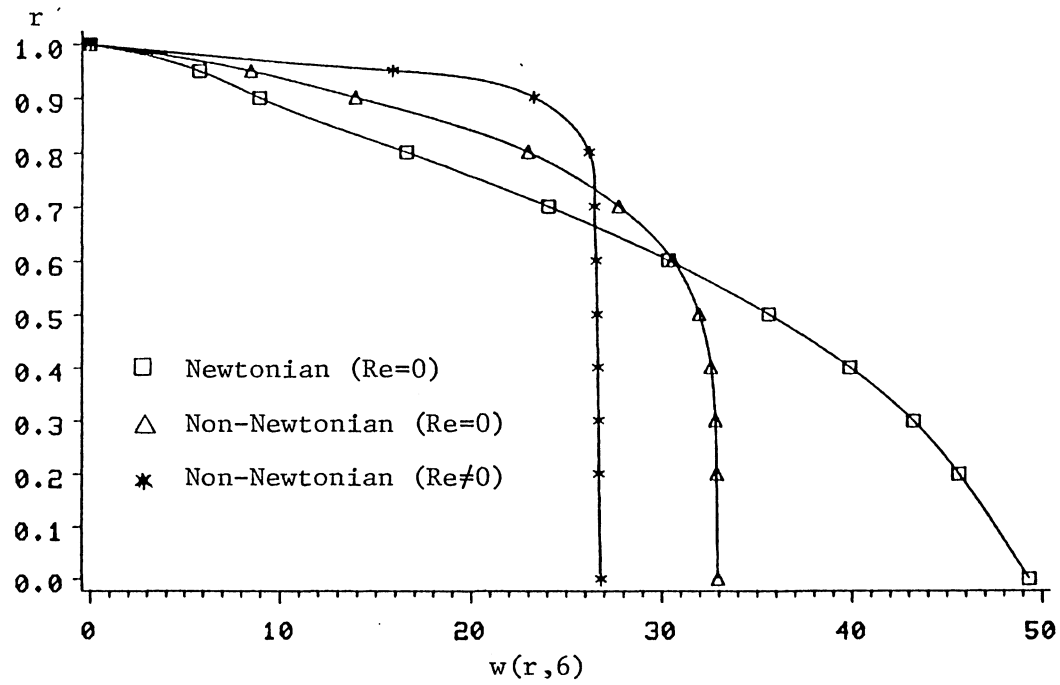


Figure 14. Velocity profiles for a power-law fluid in a pipe
 $(w_0=25.0, n=0.2, \eta_0=1.0, R=1.0, \eta_1=\eta_2, L=6.0)$

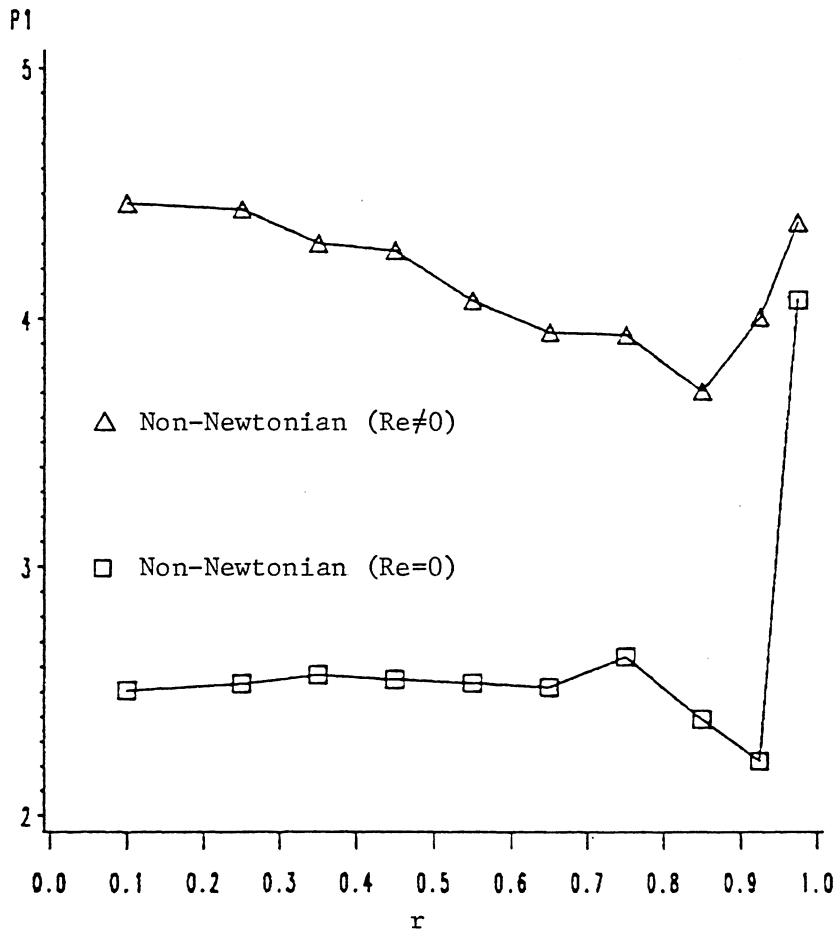


Figure 15. Pressure profiles for a power-law fluid in a pipe ($w_0=25.0$)

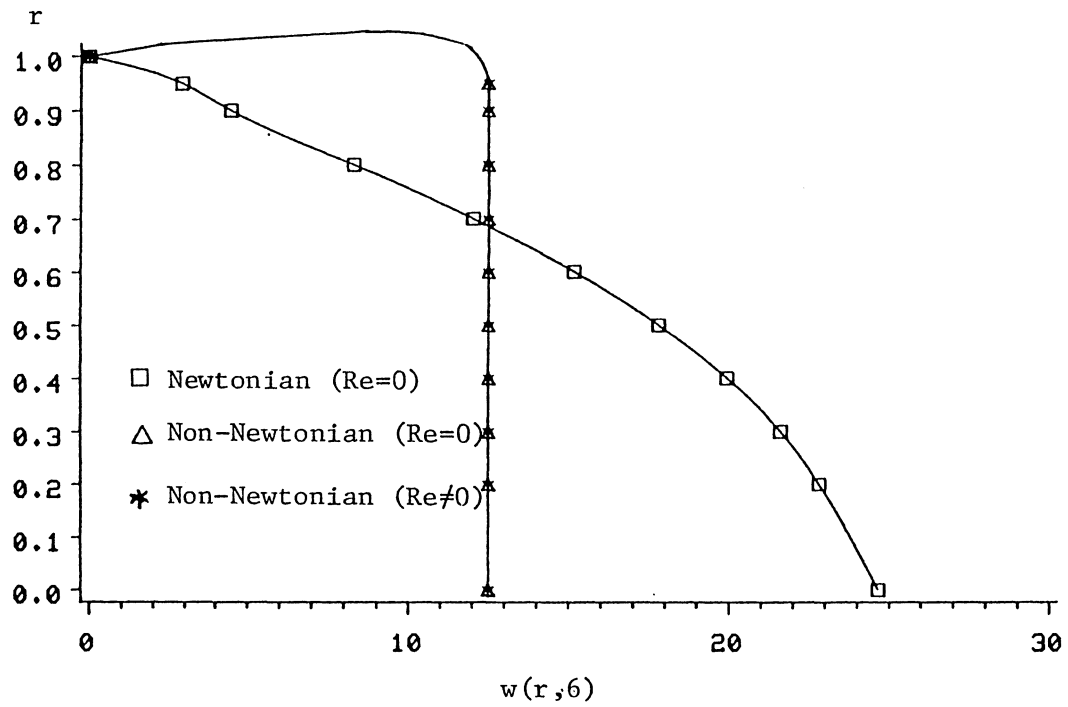


Figure 16. Velocity profiles for a power-law fluid through a pipe ($w_0=12.5$, $n=-0.6$, $R=1.0$, $L=6.0$, $\eta_0=1.0$, $\eta_1=\eta_2$)

rate through the tube shows similar behavior, as can be seen from the plots in Figure 17.

Lastly, flow through a 4 to 1 tubular contraction is analyzed. The geometry ($L_1 = 10$, $L_2 = 6$, $R_1 = 4$, and $R_2 = 1$), boundary conditions and mesh are shown in Figures 2 and 4. Fully developed flow is assumed at the entry and exit region. The results presented here are for the power-law fluids with $n = 0.5$ and $n = 0.2$. The inertial effects are considered and compared as before. Figure 18 shows the development of axial velocity along the axis of symmetry for unit downstream radius and flow rate of π ; for $n = 0.5$, the results obtained are in excellent agreement with the results published by Crochet [44]. The comparison for inertial effects is also shown in Figure 18. The magnitude of velocity decreases a little. Other than that the solution is not affected. Figures 19 and 20 contain the streamlines for these two cases. Streamlines do not seem to be affected by inertial terms. Figure 21 contains the velocity profile for the power-law fluid with $n = 0.2$. The plot is similar to that obtained for the power-law fluid with $n = 0.5$ and the same comments are valid.

4.2.6 Analysis of White-Metzner Fluids

It has been recommended by other researchers [38] that for White-Metzner model, the viscosities η_1 and η_2 should be the fractions of shear viscosity η where $\eta_2/\eta_1 \geq \frac{1}{8}$. The results presented here are obtained using $\eta_2/\eta_1 = \frac{1}{8}$.

The same geometries as used before are considered for the White-Metzner fluid. Flow through a plane channel with unit shear viscosity

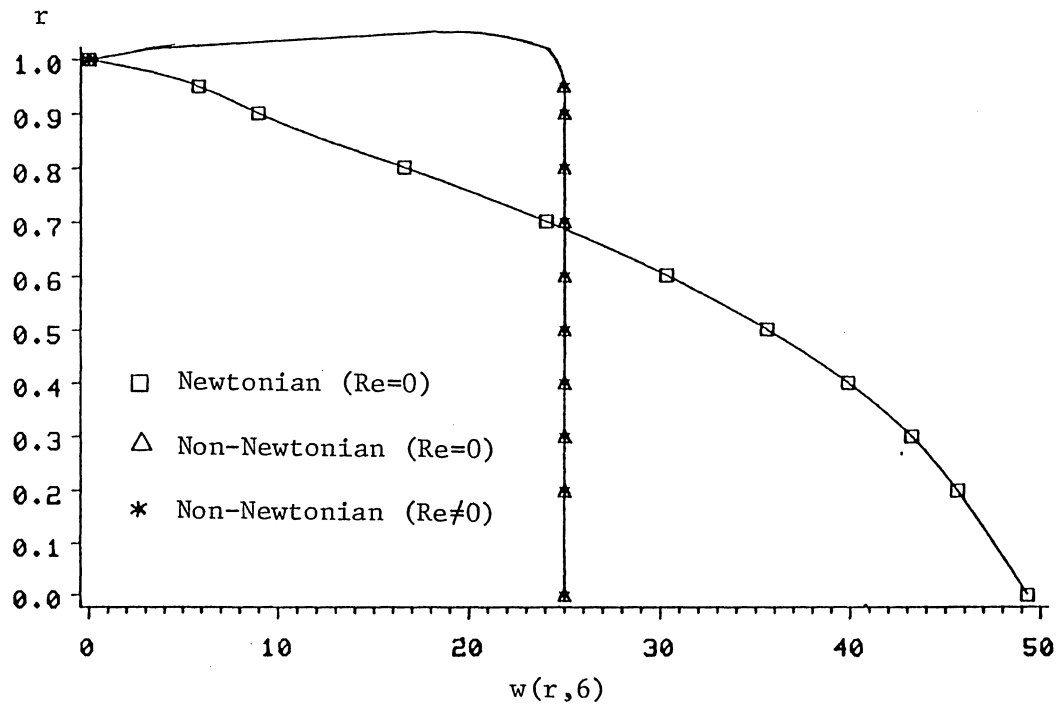


Figure 17. Velocity profiles for a power-law fluid through a pipe ($w_0=25.0$, $n=-0.6$, $R=1.0$, $L=6.0$, $\eta_0=1.0$, $\eta_1=\eta_2$)

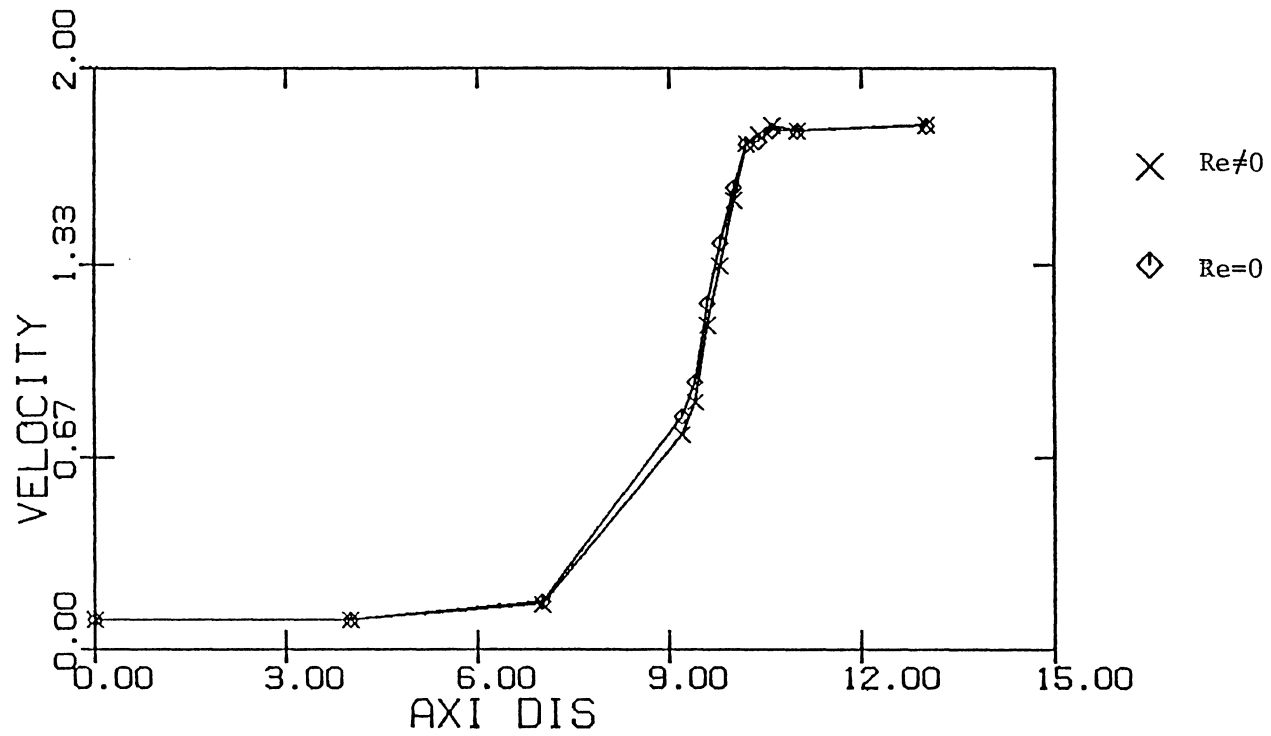


Figure 18. Velocity profiles for a power-law fluid through a 4 to 1 tubular contraction (flow rate= π , $n=0.5$, $R_1=4$, $R_2=1$, $L_1=10$, $L_2=6$, $\eta_0=1.0$, $\eta_2=0$)

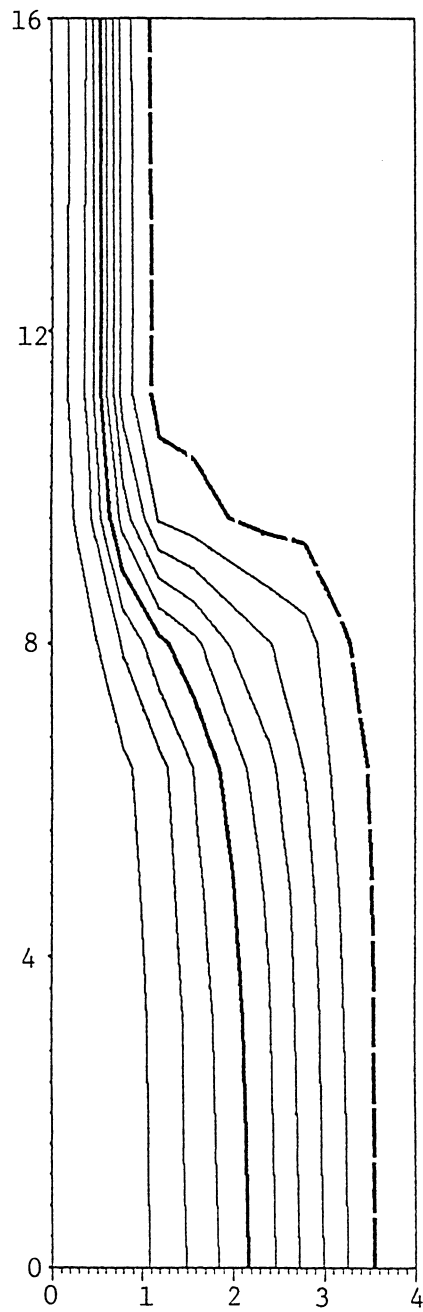


Figure 19. Streamlines for a power-law fluid through a 4 to 1 tubular contraction ($n=0.5$, $Re=0$)

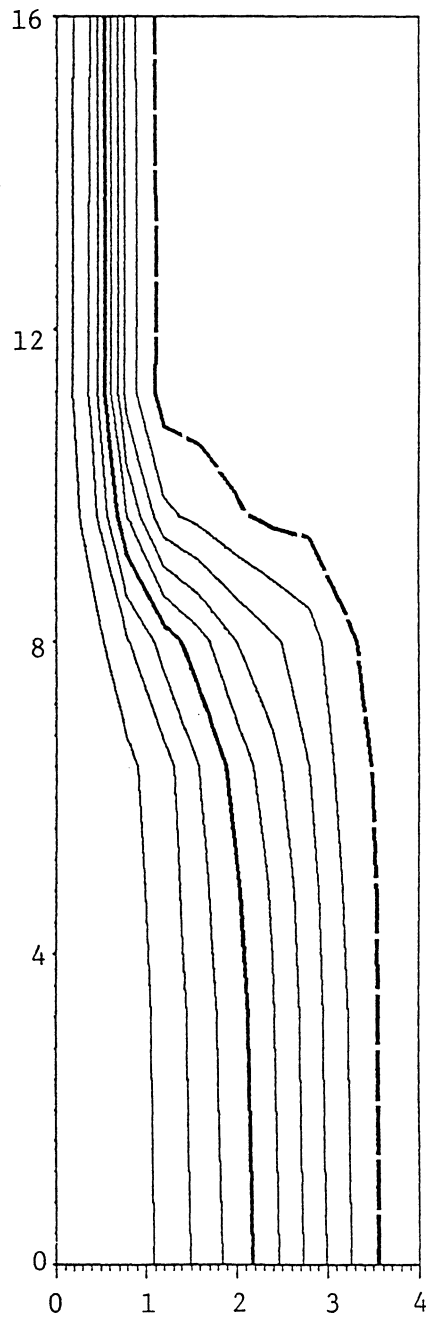


Figure 20. Streamlines for a power-law fluid through a 4 to 1 tubular contraction ($n=0.5$, $Re \neq 0$)

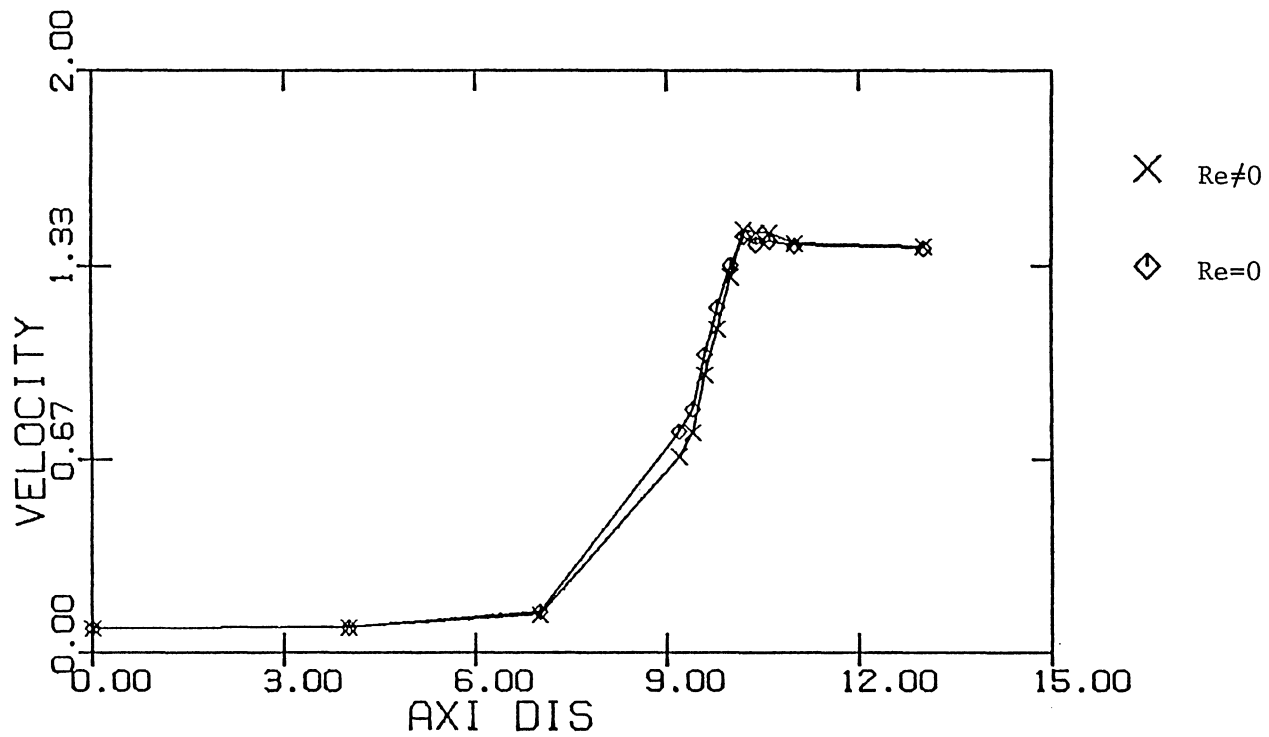


Figure 21. Velocity profiles for a power-law fluid through a 4 to 1 tubular contraction (flow-rate= π , $n=0.2$, $R_1=4$, $R_2=1$, $L_1=10$, $L_2=6$, $\eta_0=1.0$, $\eta_2=0$)

and unit flow rate is considered. The geometry, mesh and boundary condition are shown in Figures 1 and 4. Figure 22 shows the velocity profile for Newtonian fluid and White-Metzner fluid with and without inertia terms. The Newtonian fluid shows a fully developed profile where as for White-Metzner fluid the profile is much flatter. Also at unit flow rate, the presence of inertia does not affect the solution. The pressure fluctuates more near the wall (see Figure 23) due to its infinite nature, and increases in value due to inertial effects. These observations are very similar to the observations made for the power-law fluid.

Flow through a channel is analyzed again with increased flow rate of 2 units and 5 units to investigate the inertial effect. Figures 24 and 25 contain the axial velocity profiles. It can be seen from Figures 24 and 25 that the inertial effects become more visible at the higher flow rate (i.e. at higher inlet velocity). The viscous effects seem to vanish and the inertial terms dominate the solution, and the velocity profile becomes flatter.

Next, a flow through a tube is considered, for the flow rate of π , 2π and 5π . The results are presented in Figures 26 thru 29. Observations similar to those made for plane channel flow can be made here.

Lastly, flow of a White-Metzner fluid through a 4 to 1 tubular and plane contraction is investigated. Fully developed flow is assumed in the entry and exit region. The fluid with unit shear viscosity and a flow rate of π is analyzed. In Figure 30 contains axial velocity profiles with and without inertia effects. These results are very

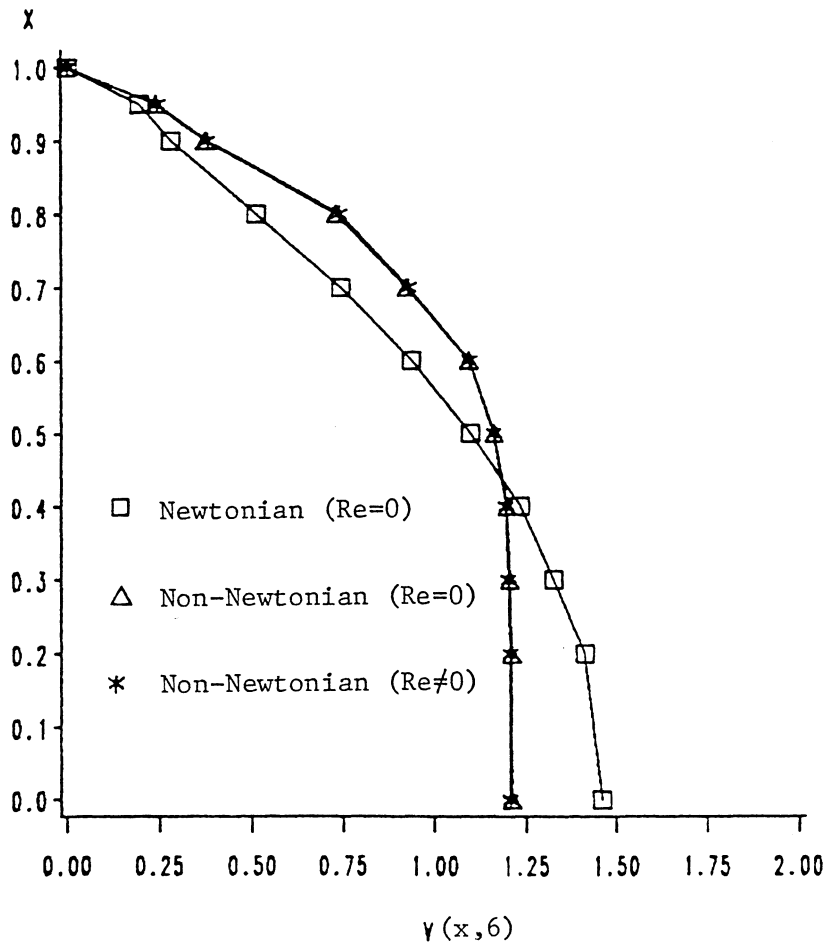


Figure 22. Velocity profiles for a White-Metzner fluid through a plane channel ($V_0=1.0$, $n=0.2$, $R=1.0$, $L=6$, $\eta_0=1.0$, $\eta_2=\eta_1/8$)

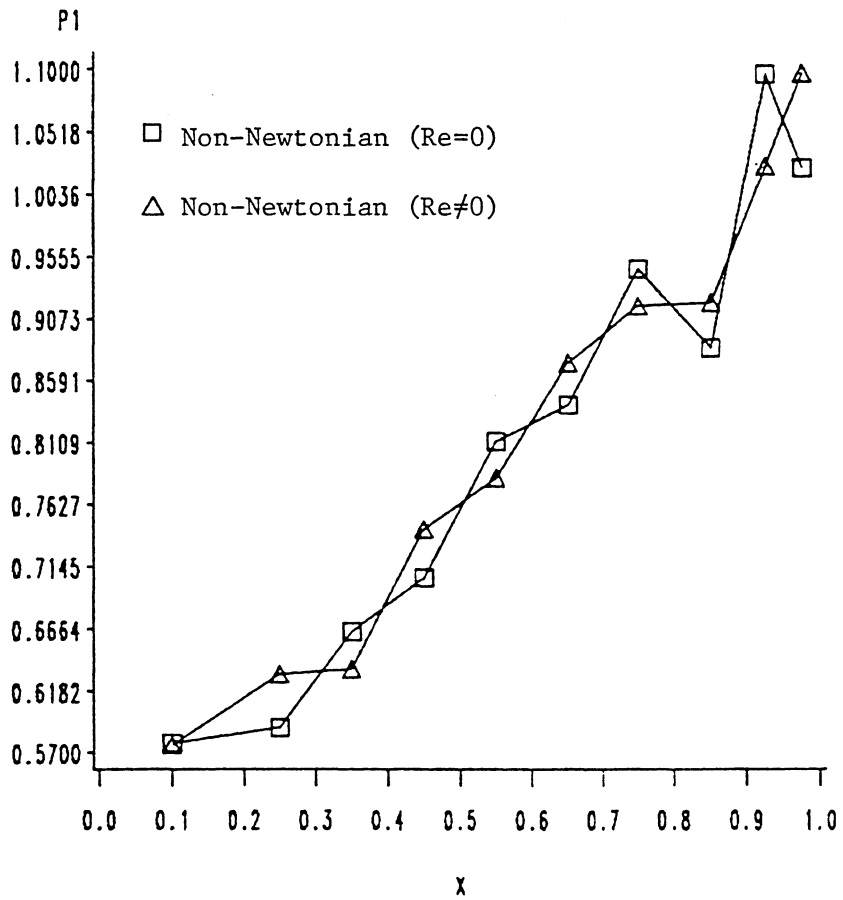


Figure 23. Pressure profiles for a White-Metzner fluid through a plane channel ($v_0=1.0$, $n=0.2$)

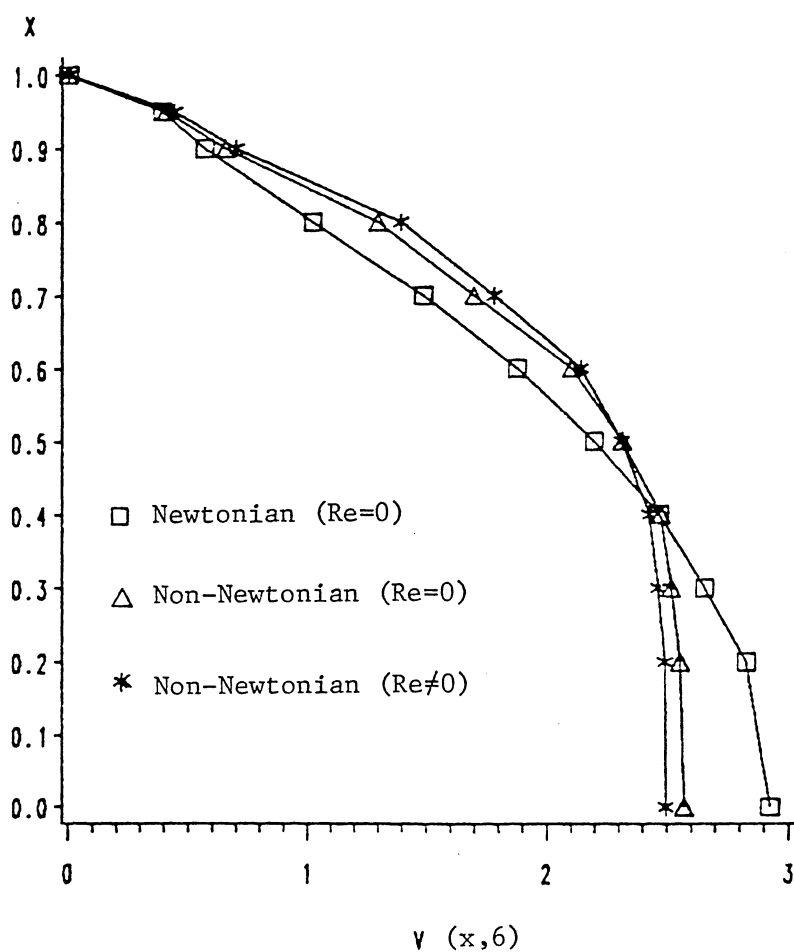


Figure 24. Velocity profiles for a White-Metzner fluid through a plane channel ($v_0=2.0$, $n=0.2$, $R=1$, $L=6$, $\eta_0=1.0$, $\eta_2=\eta_1/8$)

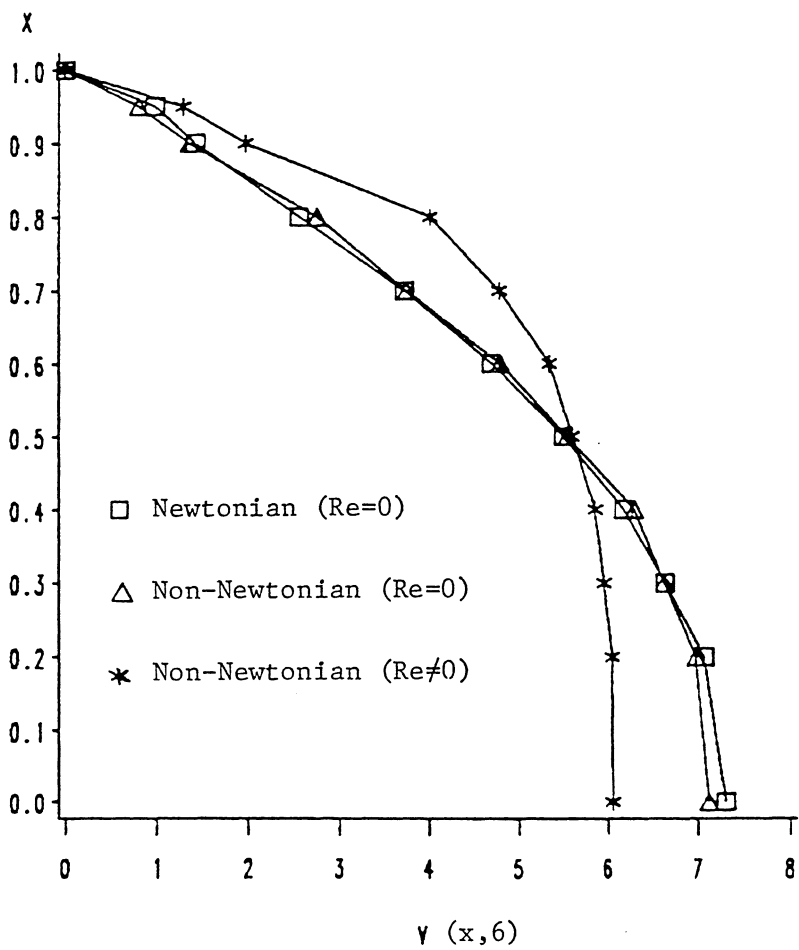


Figure 25. Velocity profiles for a White-Metzner fluid through a plane channel ($v_0=5.0$, $n=0.2$, $\eta_0=1.0$, $\eta_2=\eta_1/8$, $R=1.0$, $L=6.0$)

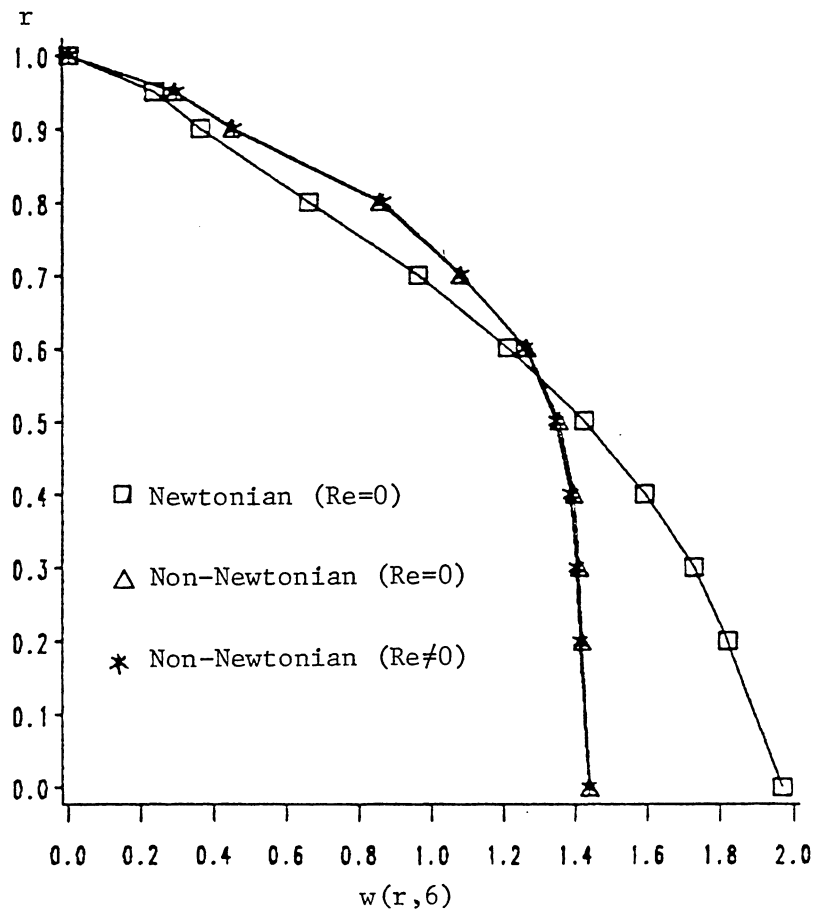


Figure 26. Velocity profiles for a White-Metzner fluid through a pipe ($w_0=1.0$, $n=0.2$, $\eta_0=1.0$, $\eta_2=\eta_1/8$, $R=1.0$, $L=6.0$)

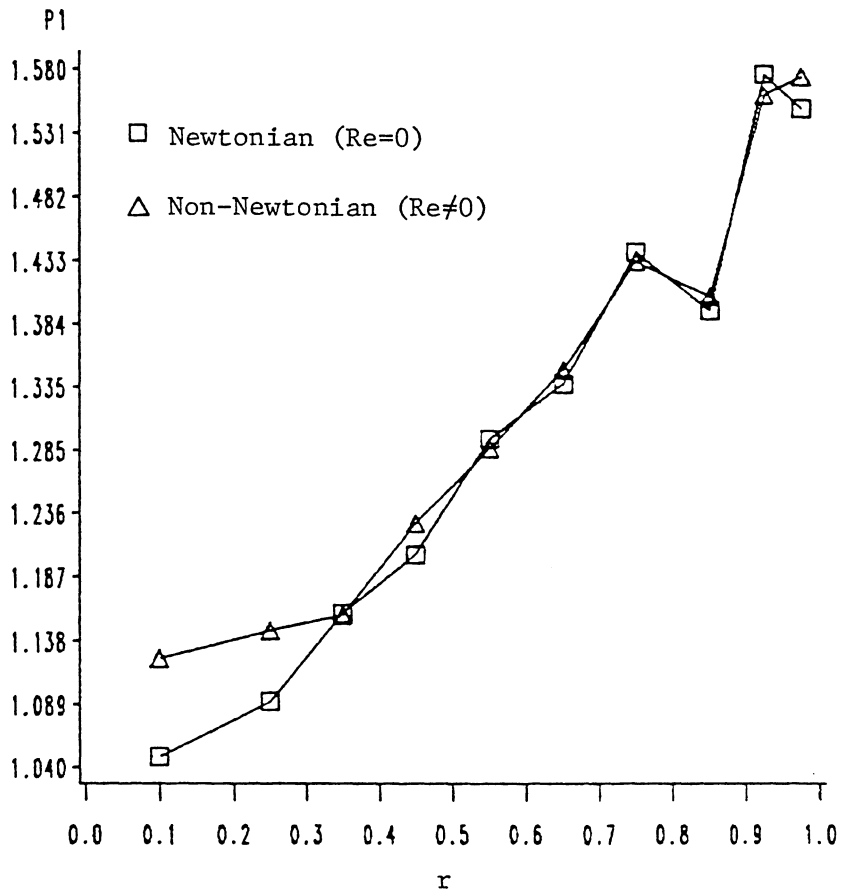


Figure 27. Pressure profiles for a White-Metzner fluid through a pipe ($w_0=1.0$, $n=0.2$)

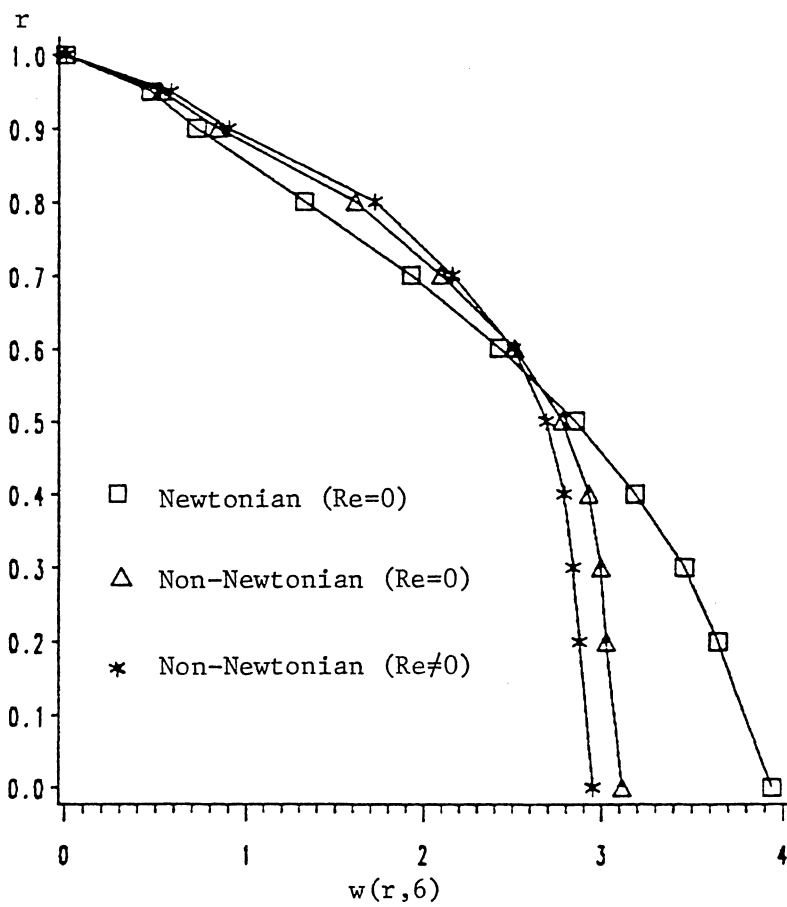


Figure 28. Velocity profiles for a White-Metzner fluid through a pipe ($w_0=2.0$, $n=0.2$, $\eta_0=1.0$, $\eta_2=\eta_1/8$, $R=1.0$, $L=6.0$)

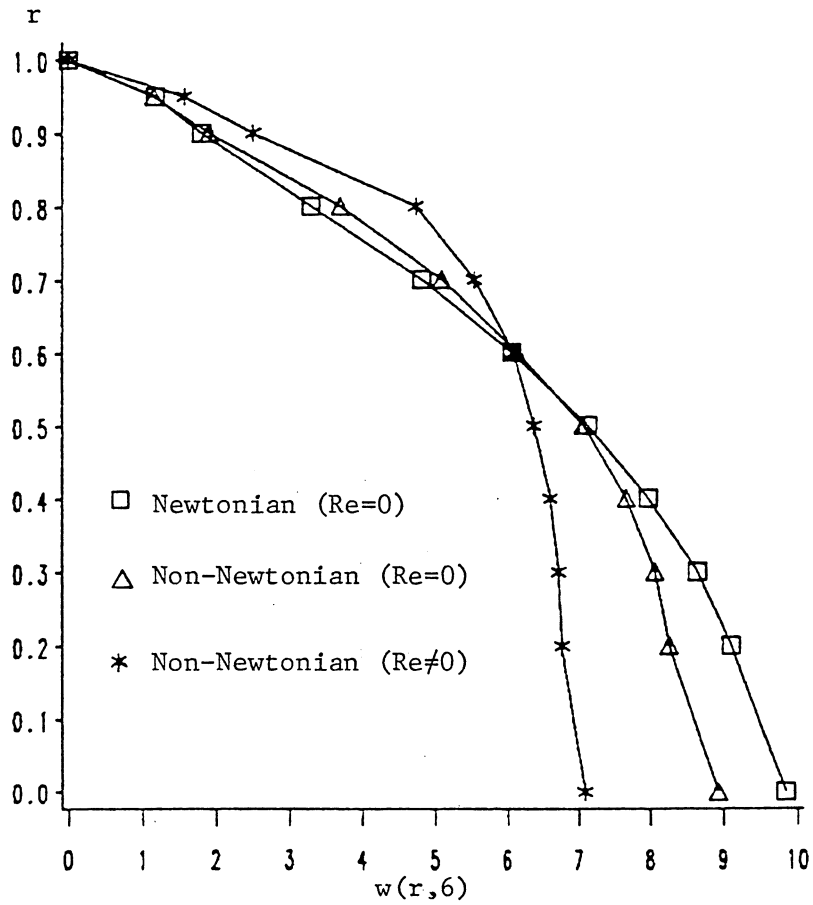


Figure 29. Velocity profiles for a White-Metzner fluid through a pipe ($w_0=5.0$, $n=0.2$, $\eta_0=1.0$, $\eta_2=\eta_1/8$, $R=1.0$, $L=6.0$)

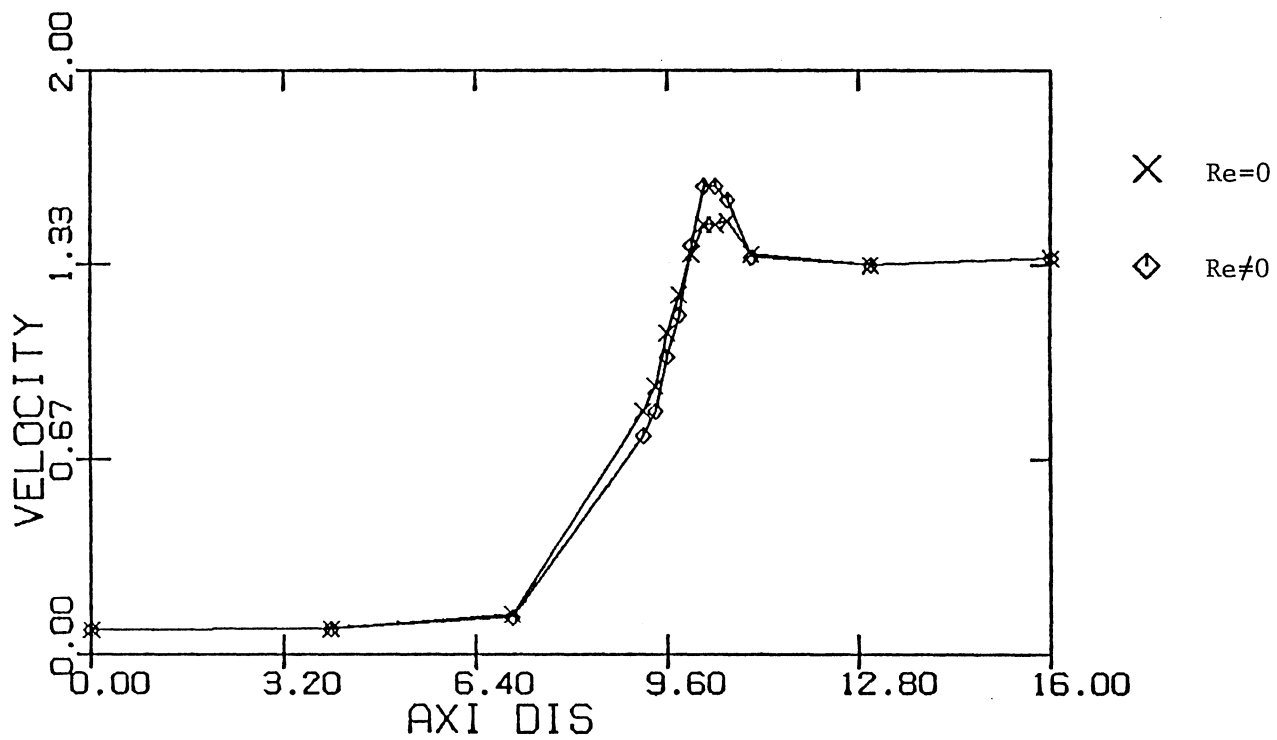


Figure 30. Velocity profiles for a White-Metzner fluid through 4 to 1 tubular contraction (flow rate= π , $n=0.2$, $\eta_0=1.0$, $\eta_2=\eta_1/8$, $R_1=4$, $R_2=1$, $L_1=10$, $L_2=6$)

similar to the results published by Crochet and Louvain [44] for Maxwell type fluids. A similar overshoot is observed near the reentry region for the White-Metzner fluid. The streamlines with and without inertia terms are presented in Figure 31 and Figure 32. The inertia does not affect the streamlines. The secondary flow in the corner is not seen in Figures 31 and 32, but the velocity solution proves its presence by negative velocity components.

For the plane flow, the problem is the same except that a unit flow rate is considered. The results are presented in Figure 33 through 35. They are very similar to the result obtained for axisymmetric flow and the same comments are valid here.

4.2.7 Transient Analysis

To demonstrate the applicability of the finite element model to the transient analysis, a power-law fluid ($n = 0.2$, $\eta_0 = 1.0$, $\eta_2 = 0$) in a tube ($R = 1$, $L = 6$) is analyzed using a 10×6 uniform mesh of linear elements with time step, $\Delta t = 0.01$. The results of various solutions obtained are compared in Fig. 36. The effects of inertia and non-Newtonian constitutive relations are brought out in these plots. Like in the steady-state solutions, the effect of using the power-law constitutive equation on the axial velocity is to flatten the profile at the exit (from a parabolic one for Stokes and Navier-Stokes fluids). The inertia seems to stabilize the velocity field (relative to the Stokes solution) of power-law fluids. Also, the power-law fluids take quite a long time to develop to the steady-state solution when compared to the Newtonian fluids.

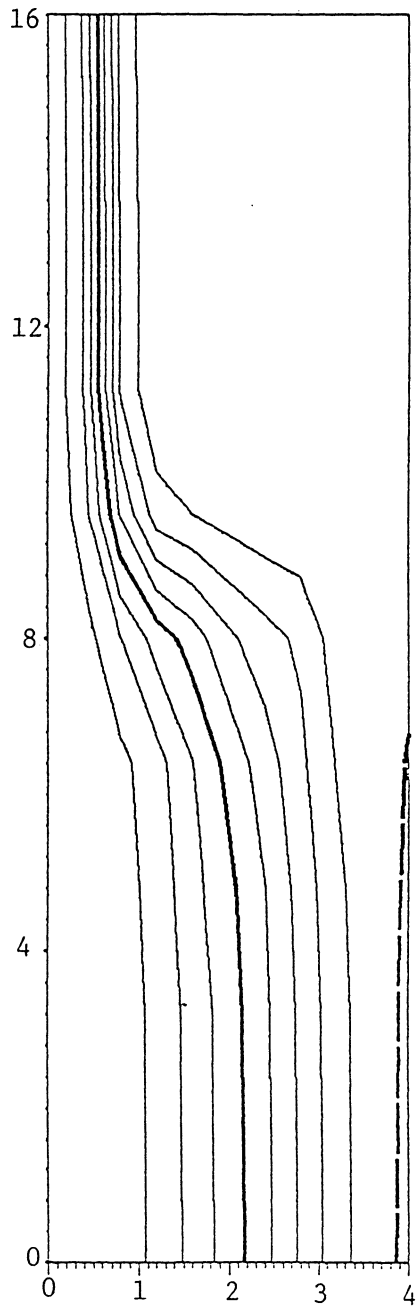


Figure 31. Streamlines for a White-Metzner fluid in a 4 to 1 tubular contraction ($n=0.2$, $Re=0$)

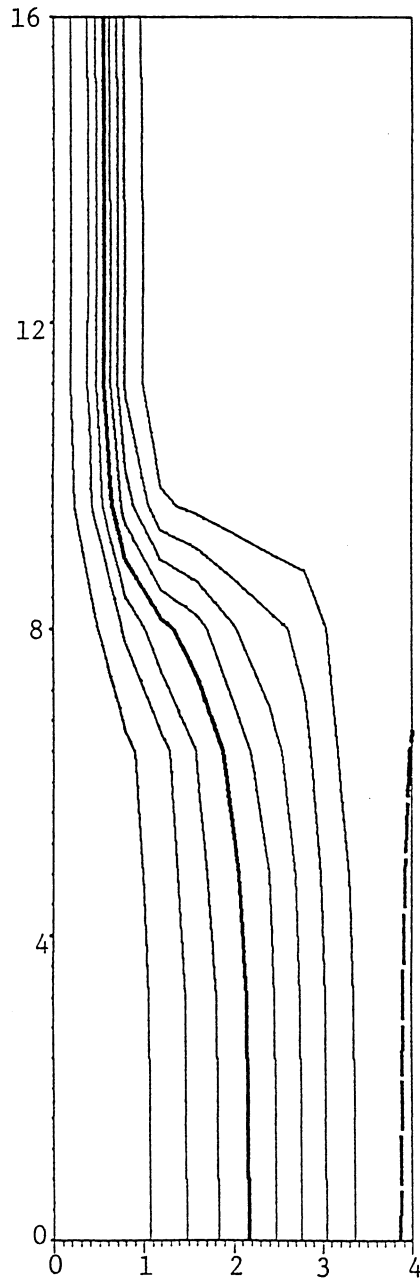


Figure 32. Streamlines for a White-Metzner fluid in a 4 to 1 tubular contraction ($n=0.2$, $Re \neq 0$)

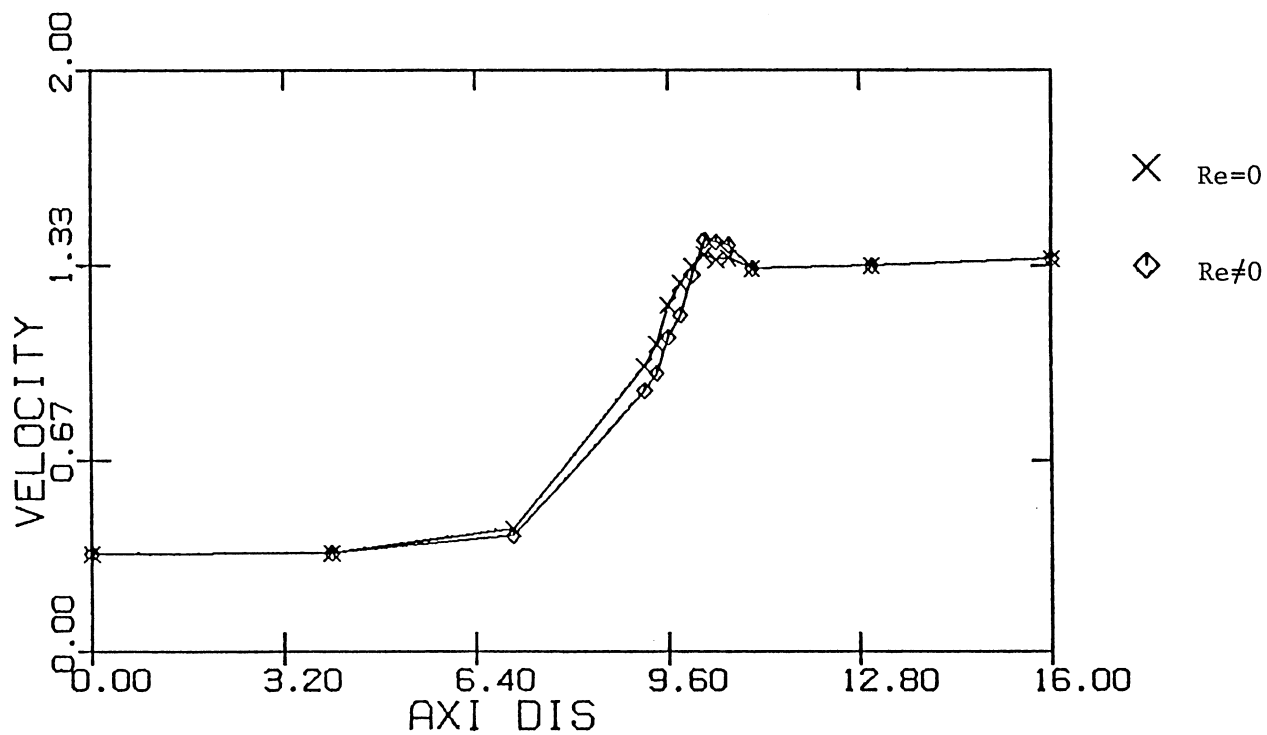


Figure 33. Velocity profiles for a White-Metzner fluid through a 4 to 1 contraction channel (flow rate=1.0, $n=0.2$, $\eta_0=1.0$, $\eta_2=\eta_1/8$, $R_1=4$, $R_2=1$, $L_1=10$, $L_2=6$)

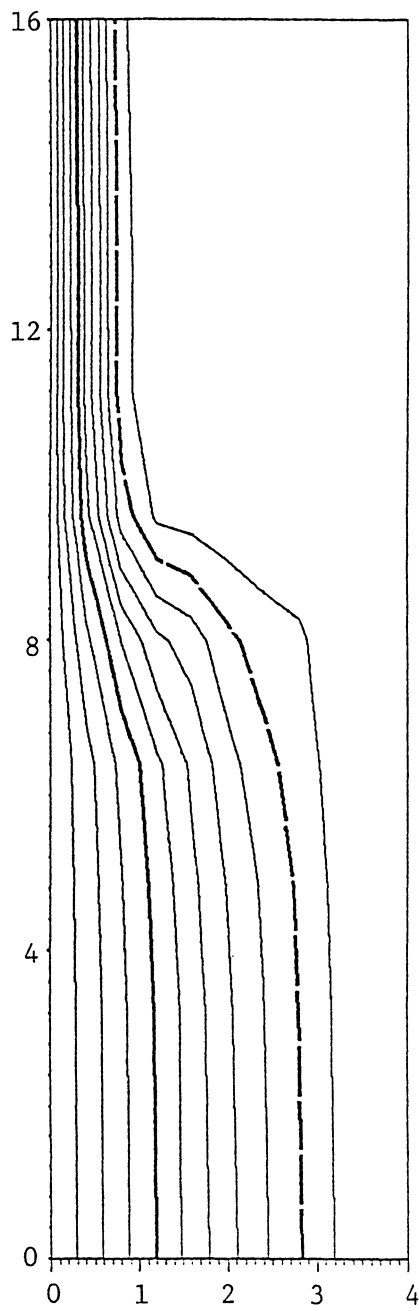


Figure 34. Streamlines for a White-Metzner fluid in a 4 to 1 contraction channel ($n=0.2$, $Re=0$)

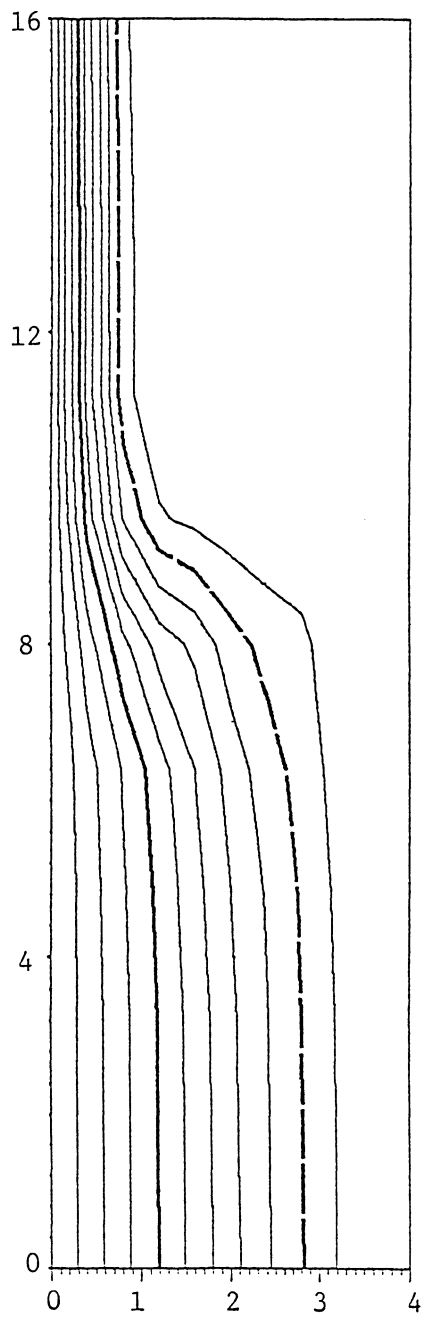


Figure 35. Streamlines for a White-Metzner fluid in a 4 to 1 contraction channel ($n=0.2$, $Re \neq 0$)

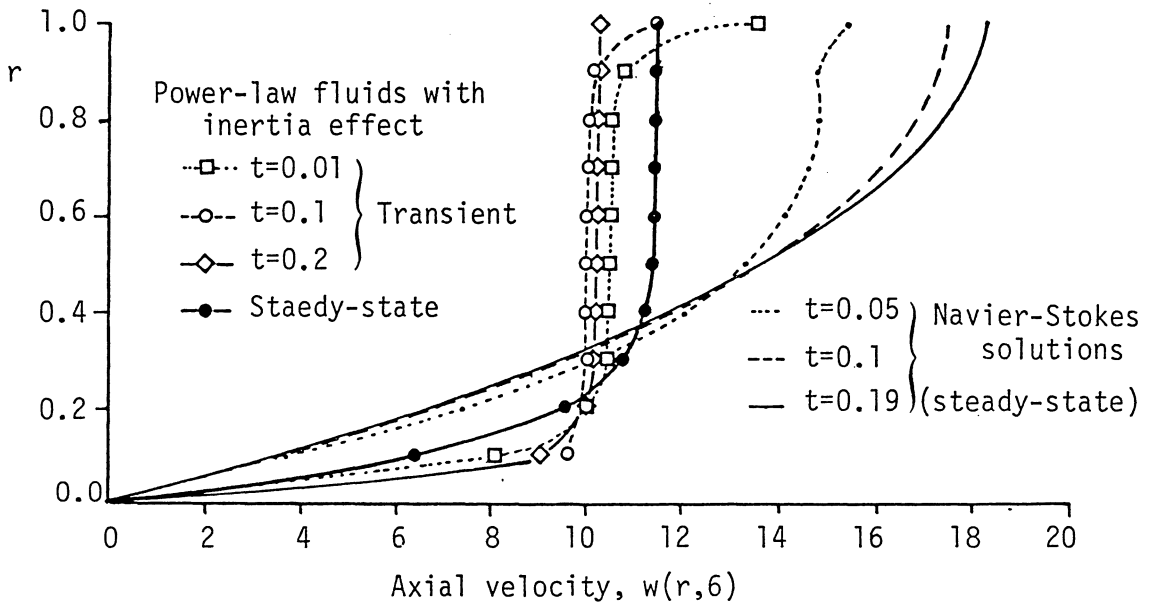
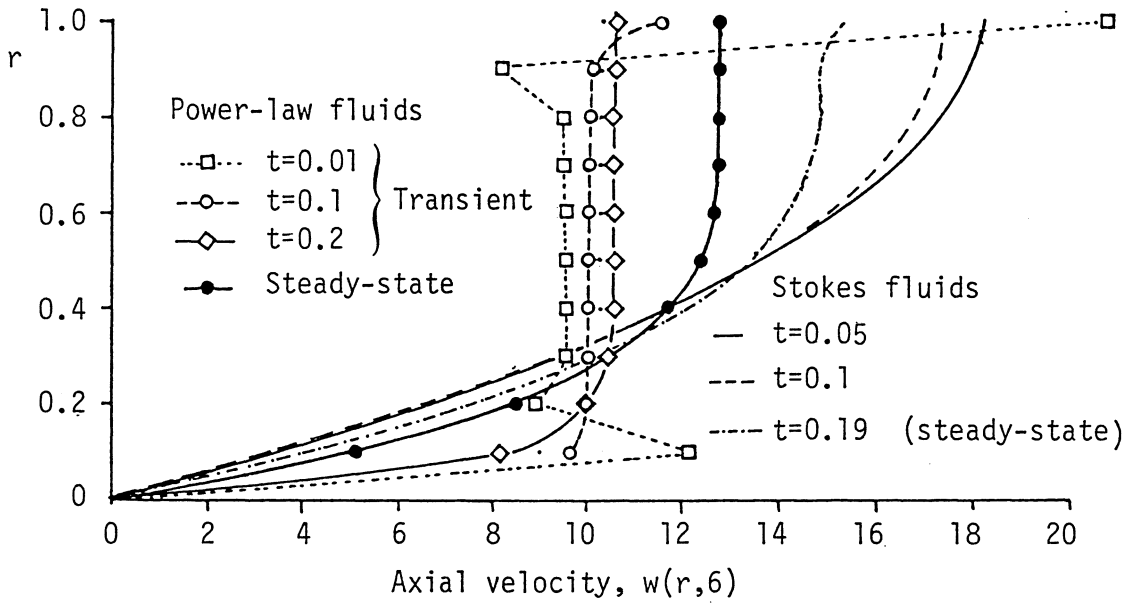


Figure 36. Transient analysis of a power-law fluid through a pipe ($R=1, L=6, n=0.2, \rho_0=1, \mu_0=0$) using the velocity finite element model (with 10×6 mesh, $\Delta t=0.01$).

CHAPTER V

CONCLUSION AND RECOMMENDATIONS

5.1 Conclusions

Velocity and mixed penalty finite element models are developed to analyze plane and axisymmetric flows of power-law and viscoelastic (White-Metzner type) fluids. The most significant features of this study are the inclusion of the inertia (or convective) terms and transient analysis. The primary focus of this study has been the development of a numerical model of the flows of power-law and White-Metzner fluids. No attempt is made to validate or invalidate the constitutive models, but accepted them to evaluate the effects of inertia and transient response in axisymmetric flow situations. The model can also be used to analyze the flows of Newtonian and other power-law (e.g., Correau model) fluids. The penalty parameter, in the range $\gamma_p = 10^6 - 10^{12}$, is found to yield converged solutions for the problems studied here. For power-law fluids, specification of stress components at the entry region does not affect the solution when the mixed model is used. The White-Metzner type fluids require the specification of all extra stress components at the entry region. Otherwise, the solution does not converge.

At higher Reynolds number, the inertial effects become dominant for both power-law and White-Metzner fluids. Neglecting the inertia effect at high Reynolds number can result significant error in the solution; and hence should not be neglected.

5.2 Recommendations

The Penalty finite element models developed here can be easily extended to analyze other viscoelastic models like Maxwell, Oldroyd, Gieskus, etc. The approximation functions used in the present study are Lagrange linear and quadratic approximation functions like Hermite cubics can also be used to obtain a smoother solution, especially in the case of the contraction problem. Also, the Picard type iterative procedure can be substituted by Newton Raphson technique which is known to converge faster and is more efficient. Also, the models can be extended to study physical processes involving non-Newtonian fluids in the presence of thermal gradients.

REFERENCES

1. O. C. Zienkiewicz, and Y. K. Cheung, "Finite elements in the solution of field problems," The Engineer, Vol. 220, pp. 507-510, 1965.
2. J. T. Oden, "A finite element analogue of the Navier-Stokes equations," J. Engng. Mech. Div., ASCE, Vol. 96(EM4), pp. 529-534, 1970.
3. J. T. Oden, and D. Somogyi, "Finite element applications in fluid dynamics," J. Engng. Mech. Div., ASCE, Vol. 95(EM4), pp. 821-826, 1969.
4. J. T. Oden, and Wellford, Jr. L. C., "Analysis of flow of viscous fluids by the finite element method," AIAA J., Vol. 10(12), pp. 1590-1599, 1972.
5. J. H. Argyris, G. Mareczek, and D. W. Scharpf, "Two- and three-dimensional flow using finite elements," The Aero, J. Roy. Aero. Soc., vol. 73, pp. 961-964, 1969.
6. P. Tong, "The finite element method for fluid flow," In: R. H. Gallagher et al. (Editors), Matrix Methods of Structural Analysis and Design, University of Alabama Press, Huntsville, Ala., pp. 787-808, 1971.
7. R. T. Cheng, "Numerical solution of the Navier-Stokes equations by the finite element method," The Physics of Fluids, Vol. 14(12), pp. 2098-2105, 1972.
8. M. D. Olson, "A variational finite element method for two-dimensional steady viscous flows," Joint McGill University-Engineering Institute of Canada Conference on Finite Element Methods in Civil Engineering, Montreal, 1972.
9. A. J. Baker, "Finite element theory for viscous fluid dynamics," Bell Aerospace Co. Report No. 9500-920189.
10. A. J. Baker, "Finite element solution algorithm for viscous incompressible fluid dynamics," Int. J. Numer. Meth. Engr., Vol. 6, pp. 89-101, 1973.
11. C. Taylor, and P. Hood, "A numerical solution of the Navier-Stokes equations using the finite element technique," Computers and Fluids, Vol. 1, pp. 73-100, 1973.

12. M. Kawahara, N. Yoshimura, and K. Nakagawa, "Analysis of steady incompressible viscous flow," In: J. T. Oden et al. (Editors), Finite Element Methods in Flow Problems, UAH Press, Huntsville, Alabama, pp. 107-120, 1974.
13. M. D. Olson, "Variational-finite element methods for two-dimensional and axisymmetric Navier-Stokes equations," In: J. T. Oden et al. (Editors), Finite Element Methods in Flow Problems, UAH Press, Huntsville, Alabama, pp. 103-106, 1974.
14. G. De Vahl Davis, "Laminar natural convection in an enclosed rectangular cavity," Int. J. Heat Mass Transfer, Vol. 11, pp. 1675-1693, 1968.
15. M. D. Olson and S. Y. Tuann, "A study of various finite element solution methods for the Navier-Stokes equations," Structures Report No. 14, Department of Civil Engineering, University of British Columbia, Vancouver, 1976.
16. J. N. Reddy, "On the accuracy and existence of solutions to primitive variable models of viscous incompressible fluids," Int. J. Engng. Sci., Vol. 16, pp. 921-929, 1978.
17. J. N. Reddy, Applied Functional Analysis and Variational Methods in Engineering, McGraw-Hill, New York, 1986.
18. O. C. Zienkiewicz, "Constrained variational principles and penalty analysis function methods in finite elements," Conf. on Numerical Solution of Differential Equations, Dundee. Lecture Notes on Mathematics, 1973, Springer.
19. T. J. R. Hughes, R. L. Taylor, and J. F. Levy, "A finite element method for incompressible viscous flows," Proceedings of the Second International Symposium on Finite Element Methods in Flow Problems, Santa Margherita Ligure, Italy, 1976.
20. J. N. Reddy, "Penalty finite element methods for the solution of advection and free convection flows," In: A. P. Kabaila and V. A. Pulmano (Editors), Finite Element Methods in Engineering, The University of New South Wales, Sydney, Australia, pp. 583-598, 1979.
21. J. N. Reddy, "On penalty function methods in the finite element analysis of fluid flow," Int. J. Numer. Meth. in Fluids, Vol. 2, 151-171, 1982.
22. J. N. Reddy, "Penalty-finite element methods in conduction and convection heat transfer," In: R. W. Lewis, K. Morgan and B. A. Schrefler (Editors), Numerical Methods in Heat Transfer, Vol. II, John Wiley, London, pp. 145-178, 1983.

23. R. I. Tanner, "Die-Swell reconsidered: some numerical solutions using a finite element program," Applied Polymer Symposium, Vol. 20, pp. 201-208, 1973.
24. R. I. Tanner, R. E. Nickell and R. W. Bilger, "Finite element methods for the solution of some incompressible non-Newtonian fluid mechanics problems with free surfaces," Comp. Meth. Appl. Mech. Engng., Vol. 6, pp. 155-179, 1975.
25. R. E. Nickell, R. I. Tanner and B. Caswell, "The solution of viscous incompressible jet and free surface flows using finite element methods," J. Fluid Mech., Vol. 65, pp. 189-206, 1974.
26. R. I. Tanner, "Some experiences using finite element methods in polymer processing and rheology," Proc. Seventh Int. Congress on Rheology, C. Klason and J. Kubat (eds.), Gotherburg, pp. 140-145, 1976.
27. K. R. Reddy and R. I. Tanner, "Finite element approach to die-swell problems of non-Newtonian fluids," Proc. 6th Australian Hydraulics and Fluid Mechanics Conference, pp. 431-434, 1977.
28. B. Caswell and R. I. Tanner, "Wirecoating die design using finite element methods," Polymer. Engng. Sci., Vol. 18, pp. 416-421, 1978.
29. D. V. Boger, R. Gupta and R. I. Tanner, "The end-correction for power-law fluids in the capillary rheometer," J. non-Newtonian Fluid Mech., Vol. 4, pp. 239-248, 1978.
30. O. C. Zienkiewicz, P. C. Jain and E. Onate, "Flow of solids during forming and extrusion: some aspects of numerical solutions," International Journal of Solids and Structures, Vol. 14, pp. 15-38, 1978.
31. O. C. Zienkiewicz and P. N. Godbole, "Viscous, incompressible flow with special reference to non-Newtonian (plastic) fluids," Finite Element Method in Flow Problems, (Edited by R. A. Gallagher, J. T. Oden, C. T. Taylor and O. C. Zienkiewicz) Chapter 2, Wiley, New York, 1975.
32. P. W. Chang, T. W. Patten and B. A. Finlayson, "Collocation and Galerkin finite element methods for viscoelastic fluid flow," Computers and Fluids, Vol. 7, pp. 267-293, 1979.
33. M. Kawahara and N. Takeuchi, "Mixed finite element method for analysis of viscoelastic fluid flow," Computers and Fluids, Vol. 5, pp. 33-45, 1977.
34. M. J. Crochet and M. Bezy, "Numerical solution for the flow of viscoelastic fluids," Journal of Non-Newtonian Fluid Mechanics, Vol. 5, pp. 201-218, 1979.

35. C. J. Coleman, "A finite element routine for analyzing non-Newtonian fluids, Part 1," Journal of Non-Newtonian Fluid Mechanics, Vol. 7, pp. 289-301, 1980.
36. G. D. Richards and P. Townsend, "A finite element computer model of the hole pressure problem," Rheol. Acta, Vol. 20, pp. 261-269, 1981.
37. A. R. Davies, S. J. Lee and M. F. Webster, "Numerical simulation of viscoelastic flow: The effect of mesh size," Journal of Non-Newtonian Fluid Mechanics, 1983.
38. M. J. Crochet, A. R. Davies and K. Walters, Numerical Simulation of Non-Newtonian Flow, Elsevier, Amsterdam, 1984.
39. J. L. White and A. B. Metzner, "Development of constitutive equations for polymeric melts and solutions," Journal of Applied Polymer Science, Vol., pp. *-*, 1963.
40. M. Read, "An experimental and numerical analysis of the exit flow in a slit die for polymer melts," Ph.D. Thesis, Department of Chemical Engineering, Virginia Polytechnic Institute and State University, Blacksburg, VA, March 1986.
41. A. Gotsis, "Numerical simulation of viscoelastic flow: effect of the rheological model and the mesh," Ph.D. Thesis, Virginia Polytechnic Institute and State University, Blacksburg, VA 24060, September, 1986.
42. R. B. Bird, W. E. Stewart and E. N. Lightfoot, Transport Phenomenon, Wiley, New York, 1960.
43. J. N. Reddy, An Introduction to the Finite Element Method, McGraw-Hill, New York, 1984.
44. M. J. Crochet, "Finite elements for solving non-Newtonian flow," Lecture Series 1981-6, Von Karman Institute for Fluid Dynamics, Chaussee de Waterloo, 72, B-1640 Rhode St. Genese, Belgium, May 4-8, 1981.

APPENDIX A

MATRIX COEFFICIENTS FOR PLANE FLOW

The elements of the stiffness and mass metrics in Eqn. (3.8) are given by,

$$K_{ij}^{11} = \int_{\Omega^e} \left[\rho \psi_i \left(\bar{u} \frac{\partial \psi_j}{\partial x} + \bar{v} \frac{\partial \psi_j}{\partial y} \right) + \eta_2 \left(2 \frac{\partial \psi_i}{\partial x} \frac{\partial \psi_j}{\partial x} + \frac{\partial \psi_i}{\partial y} \frac{\partial \psi_j}{\partial y} \right) \right] dx dy + \gamma_p \int_{\Omega^e} \frac{\partial \psi_i}{\partial x} \frac{\partial \psi_j}{\partial x} dx dy$$

$$K_{ij}^{12} = \int_{\Omega^e} \left[\eta_2 \frac{\partial \psi_i}{\partial y} \frac{\partial \psi_j}{\partial x} \right] dx dy + \gamma_p \int_{\Omega^e} \frac{\partial \psi_i}{\partial x} \frac{\partial \psi_j}{\partial y} dx dy$$

$$K_{ij}^{13} = \int_{\Omega^e} \frac{\partial \psi_i}{\partial x} \psi_j dx dy$$

$$K_{ij}^{14} = 0$$

$$K_{ij}^{15} = \int_{\Omega^e} \frac{\partial \psi_i}{\partial y} \psi_j dx dy$$

$$K_{ij}^{21} = \int_{\Omega^2} \left[\eta_2 \frac{\partial \psi_j}{\partial y} \frac{\partial \psi_i}{\partial x} \right] dx dy + \gamma_p \int_{\Omega^e} \frac{\partial \psi_i}{\partial y} \frac{\partial \psi_j}{\partial x} dx dy$$

$$K_{ij}^{22} = \int_{\Omega^e} \left[\rho \psi_i \left(\bar{u} \frac{\partial \psi_j}{\partial x} + \bar{v} \frac{\partial \psi_j}{\partial y} \right) + \eta_2 \left(\frac{\partial \psi_i}{\partial x} \frac{\partial \psi_j}{\partial x} + 2 \frac{\partial \psi_i}{\partial y} \frac{\partial \psi_j}{\partial y} \right) \right] dx dy + \gamma_p \int_{\Omega^e} \frac{\partial \psi_i}{\partial y} \frac{\partial \psi_j}{\partial y} dx dy$$

$$K_{ij}^{23} = 0$$

$$K_{ij}^{24} = \int_{\Omega^e} \frac{\partial \psi_i}{\partial y} \psi_j \, dx dy$$

$$K_{ij}^{25} = \int_{\Omega^e} \frac{\partial \psi_i}{\partial x} \psi_j \, dx dy$$

$$K_{ij}^{31} = \int_{\Omega^e} -2 \eta_1 \psi_1 \frac{\partial \psi_j}{\partial x} \, dx dy$$

$$K_{ij}^{32} = 0$$

$$K_{ij}^{33} = \int_{\Omega^e} \left\{ \psi_i \psi_j + \lambda \psi_i \left(\bar{u} \frac{\partial \psi_j}{\partial x} + \bar{v} \frac{\partial \psi_j}{\partial y} \right) - \lambda \psi_i \left(2 \frac{\partial \bar{u}}{\partial x} \right) \psi_j \right\} dx dy$$

$$K_{ij}^{34} = 0$$

$$K_{ij}^{35} = \int_{\Omega^e} \left\{ \psi_1 \psi_j + \lambda \psi_i \left(\bar{u} \frac{\partial \psi_j}{\partial x} + \bar{v} \frac{\partial \psi_j}{\partial y} \right) - \lambda \psi_i \left(2 \frac{\partial \bar{u}}{\partial x} \right) \psi_j \right\} dx dy$$

$$K_{ij}^{34} = 0$$

$$K_{ij}^{35} = \int_{\Omega^e} -2 \lambda \frac{\partial \bar{u}}{\partial y} \psi_i \psi_j \, dx dy$$

$$K_{ij}^{41} = 0$$

$$K_{ij}^{42} = \int_{\Omega} e^{-2\eta_1} \psi_i \frac{\partial \psi_j}{\partial y} dx dy$$

$$K_{ij}^{43} = 0$$

$$K_{ij}^{44} = \int_{\Omega} e^{-2\eta_1} \left[\psi_i \psi_j + \lambda \psi_i \left(\bar{u} \frac{\partial \psi_j}{\partial x} + \bar{v} \frac{\partial \psi_j}{\partial y} \right) - 2 \lambda \frac{\partial \bar{v}}{\partial y} \psi_i \psi_j \right] dx dy$$

$$K_{ij}^{45} = \int_{\Omega} e^{-2\lambda} \frac{\partial \bar{v}}{\partial x} \psi_i \psi_j dx dy$$

$$K_{ij}^{51} = \int_{\Omega} e^{-2\eta_1} \psi_i \frac{\partial \psi_j}{\partial y} dx dy$$

$$K_{ij}^{52} = \int_{\Omega} e^{-2\eta_1} \psi_i \frac{\partial \psi_j}{\partial x} dx dy$$

$$K_{ij}^{53} = \int_{\Omega} e^{-2\lambda} \frac{\partial \bar{v}}{\partial x} \psi_i \psi_j dx dy$$

$$K_{ij}^{54} = \int_{\Omega} e^{-2\lambda} \frac{\partial \bar{u}}{\partial y} \psi_i \psi_j dx dy$$

$$K_{ij}^{55} = \int_{\Omega} e^{-2\eta_1} \left\{ 2 \psi_i \psi_j - 2 \lambda \psi_i \left(\bar{u} \frac{\partial \psi_j}{\partial x} + \bar{v} \frac{\partial \psi_j}{\partial y} \right) \right.$$

$$- 2 \lambda \left(\frac{\partial \bar{v}}{\partial y} + \frac{\partial \bar{u}}{\partial x} \right) \psi_i \psi_j \} dx dy$$

$$M_{ij}^{11} = \int_{\Omega^e} \rho \psi_i \psi_j dx dy \quad ; \quad M_{ij}^{1k} = 0 \quad , \quad k \neq 1$$

$$M_{ij}^{22} = \int_{\Omega^e} \rho \psi_i \psi_j dx dy \quad ; \quad M_{ij}^{2k} = 0 \quad , \quad k \neq 2$$

$$M_{ij}^{33} = \int_{\Omega^e} \lambda \psi_i \psi_j dx dy \quad ; \quad M_{ij}^{3k} = 0 \quad , \quad k \neq 3$$

$$M_{ij}^{44} = \int_{\Omega^e} \lambda \psi_i \psi_j dx dy \quad ; \quad M_{ij}^{4k} = 0 \quad , \quad k \neq 4$$

$$M_{ij}^{55} = \int_{\Omega^e} \lambda \psi_i \psi_j dx dy \quad ; \quad M_{ij}^{5k} = 0 \quad , \quad k \neq 5$$

APPENDIX B

MATRIX COEFFICIENTS FOR AXISYMMETRIC FLOW

The elements of the stiffness and mass matrices in Eqn. (3.12) are given by,

$$K_{ij}^{11} = \int_{\Omega^e} \left[\rho \psi_i \left(\bar{u} \frac{\partial \psi_j}{\partial r} + \bar{w} \frac{\partial \psi_j}{\partial z} \right) + \eta_2 \left(2 \frac{\partial \psi_i}{\partial r} \frac{\partial \psi_j}{\partial r} + \frac{\partial \psi_i}{\partial z} \frac{\partial \psi_j}{\partial z} + \frac{2}{r^2} \psi_i \psi_j \right) \right] r dr dz + \gamma_p \int_{\Omega^e} \left(\frac{\partial \psi_i}{\partial r} + \frac{1}{r} \psi_i \right) \left(\frac{\partial \psi_j}{\partial r} + \frac{1}{r} \psi_j \right) r dr dz$$

$$K_{ij}^{12} = \int_{\Omega^e} \eta_2 \frac{\partial \psi_i}{\partial z} \frac{\partial \psi_j}{\partial r} r dr dz + \gamma_p \int_{\Omega^e} \left(\frac{\partial \psi_i}{\partial r} + \frac{1}{r} \psi_i \right) \frac{\partial \psi_j}{\partial z} r dr dz$$

$$K_{ij}^{13} = \int_{\Omega^e} \frac{\partial \psi_i}{\partial r} \psi_j r dr dz$$

$$K_{ij}^{14} = 0$$

$$K_{ij}^{15} = \int_{\Omega^e} \frac{\partial \psi_i}{\partial z} \psi_j r dr dz$$

$$K_{ij}^{16} = \int_{\Omega^e} \frac{1}{r} \psi_i \psi_j r dr dz$$

$$K_{ij}^{21} = \int_{\Omega^e} \eta_2 \frac{\partial \psi_i}{\partial r} \frac{\partial \psi_j}{\partial z} r dr dz + \gamma_p \int_{\Omega^e} \left(\frac{\partial \psi_j}{\partial r} + \frac{1}{r} \psi_j \right) \frac{\partial \psi_i}{\partial z} r dr dz$$

$$K_{ij}^{22} = \int_{\Omega^e} \left[\rho \psi_i \left(\bar{u} \frac{\partial \psi_j}{\partial r} + \bar{w} \frac{\partial \psi_j}{\partial z} \right) + \eta_2 \left(\frac{\partial \psi_i}{\partial r} \frac{\partial \psi_j}{\partial r} \right) \right] r dr dz$$

$$+ 2 \frac{\partial \psi_i}{\partial z} \frac{\partial \psi_j}{\partial z} \} r dr dz + \gamma_p \int_{\Omega} e \frac{\partial \psi_i}{\partial z} \frac{\partial \psi_j}{\partial z} r dr dz$$

$$K_{ij}^{23} = 0$$

$$K_{ij}^{24} = \int_{\Omega} e \frac{\partial \psi_i}{\partial z} \psi_j r dr dz$$

$$K_{ij}^{25} = \int_{\Omega} e \frac{\partial \psi_i}{\partial r} \psi_j r dr dz$$

$$K_{ij}^{26} = 0$$

$$K_{ij}^{31} = \int_{\Omega} e - 2\eta_1 \psi_i \frac{\partial \psi_j}{\partial r} r dr dz$$

$$K_{ij}^{32} = 0$$

$$K_{ij}^{33} = \int_{\Omega} e - 2\eta_2 \psi_i \frac{\partial \psi_j}{\partial r} r dr dz$$

$$K_{ij}^{33} = \int_{\Omega} e \left\{ \psi_i \psi_j + \lambda \left[\psi_i \left(\bar{u} \frac{\partial \psi_j}{\partial r} + \bar{w} \frac{\partial \psi_i}{\partial z} \right) - 2 \psi_i \left(\frac{\partial \bar{u}}{\partial r} \psi_j \right) \right] \right\} r dr dz$$

$$K_{ij}^{34} = 0$$

$$K_{ij}^{35} = \int_{\Omega^e} -2 \lambda \frac{\partial \bar{u}}{\partial z} \psi_i \psi_j r dr dz$$

$$K_{ij}^{36} = 0$$

$$K_{ij}^{41} = 0$$

$$K_{ij}^{42} = \int_{\Omega^e} -2 \eta_1 \psi_i \frac{\partial \psi_j}{\partial z} r dr dz$$

$$K_{ij}^{43} = 0$$

$$K_{ij}^{44} = \int_{\Omega^e} \left\{ \psi_i \psi_j + \lambda \left[\psi_i \left(\bar{u} \frac{\partial \psi_j}{\partial r} + \bar{w} \frac{\partial \psi_j}{\partial z} \right) - 2 \frac{\partial \bar{w}}{\partial z} \psi_i \psi_j \right] \right\} r dr dz$$

$$K_{ij}^{45} = \int_{\Omega^e} -2 \lambda \frac{\partial \bar{w}}{\partial r} \psi_i \psi_j r dr dz$$

$$K_{ij}^{46} = 0$$

$$K_{ij}^{51} = \int_{\Omega^e} -2 \eta_1 \psi_i \frac{\partial \psi_j}{\partial z} r dr dz$$

$$K_{ij}^{52} = \int_{\Omega^e} -2 \eta_1 \psi_1 \frac{\partial \psi_j}{\partial r} r dr dz$$

$$K_{ij}^{53} = \int_{\Omega^e} -2 \lambda \frac{\partial \bar{w}}{\partial r} \psi_i \psi_j r dr dz$$

$$K_{ij}^{54} = \int_{\Omega^e} -2 \lambda \frac{\partial \bar{u}}{\partial z} \psi_i \psi_j r dr dz$$

$$K_{ij}^{55} = \int_{\Omega^e} 2 \left\{ \psi_i \psi_j + \lambda \left[\bar{u} \frac{\partial \psi_j}{\partial r} + \bar{w} \frac{\partial \psi_j}{\partial z} \right] - \left(\frac{\partial \bar{u}}{\partial r} + \frac{\partial \bar{w}}{\partial z} \right) \psi_i \psi_j \right\} r dr dz$$

$$K_{ij}^{56} = 0$$

$$K_{ij}^{61} = \int_{\Omega^e} -2 \eta_1 \psi_1 \frac{\psi_j}{r} r dr dz$$

$$K_{ij}^{62} = 0$$

$$K_{ij}^{63} = 0$$

$$K_{ij}^{64} = 0$$

$$K_{ij}^{65} = 0$$

$$K_{ij}^{66} = \int_{\Omega^e} \left\{ \psi_i \psi_j + \lambda \left[\psi_i \left(\bar{u} \frac{\partial \psi_j}{\partial r} + \bar{w} \frac{\partial \psi_j}{\partial z} - 2 \left(\frac{\bar{u}}{r} \right) \psi_i \psi_j \right) \right] \right\} r dr dz$$

$$M_{ij}^{11} = \int_{\Omega^e} \rho \psi_i \psi_j r dr dz, \quad M_{ij}^{1k} = 0, \quad k \neq 1$$

$$M_{ij}^{22} = \int_{\Omega^e} \rho \psi_i \psi_j r dr dz, \quad M_{ij}^{2k} = 0, \quad k \neq 2$$

$$M_{ij}^{33} = \int_{\Omega^e} \lambda \psi_i \psi_j r dr dz, \quad M_{ij}^{3k} = 0, \quad k \neq 3$$

$$M_{ij}^{44} = \int_{\Omega^e} \lambda \psi_i \psi_j r dr dz, \quad M_{ij}^{4k} = 0, \quad k \neq 4$$

$$M_{ij}^{55} = \int_{\Omega^e} \lambda \psi_i \psi_j r dr dz, \quad M_{ij}^{5k} = 0, \quad k \neq 5$$

$$M_{ij}^{66} = \int_{\Omega^e} \lambda \psi_i \psi_j r dr dz, \quad M_{ij}^{6k} = 0, \quad k \neq 6$$

The vita has been removed
from the scanned document